Computer Modeling in Engineering & Sciences

Tech Science Press

DOI: 10.32604/cmes.2021.015885

ARTICLE

Reliability Analysis of Piled Raft Foundation Using a Novel Hybrid Approach of ANN and Equilibrium Optimizer

Abidhan Bardhan[1], Priyadip Manna[1], Vinay Kumar[1], Avijit Burman[1], Bojan Žlender[2] and Pijush Samui[1,*]

[1]Department of Civil Engineering, National Institute of Technology, Patna, Bihar, India

[2]Faculty of Civil Engineering, Transportation Engineering and Architecture, University of Maribor, Maribor, Slovenia

[*]Corresponding Author: Pijush Samui. Email: pijush@nitp.ac.in

Received: 22 January 2021 Accepted: 31 May 2021

ABSTRACT

In many civil engineering projects, Piled Raft Foundations (PRFs) are usually preferred where the incoming load from the superstructures is very high. In geotechnical engineering practice, the settlement of soil layers is a critical issue for the serviceability of the structures. Thus, assessment of risk associated with the structures corresponding to the maximum allowable settlement of soils needs to be carried out in the design phase. In this study, reliability analysis of PRF based on settlement criteria is performed using a high-performance hybrid soft computing model. The new approach is an integration of the artificial neural network (ANN) and a recently developed meta-heuristic algorithm called equilibrium optimizer (EO). The concept of reliability index was used to explore the feasibility of a newly constructed hybrid model of ANN and EO (i.e., ANN-EO) against the conventional approach of calculating the probability of failure of PRF. Experimental results show that the proposed ANN-EO attained the most accurate prediction with $R^2 = 0.9914$ and RMSE = 0.0518 in the testing phase, which are significantly better than those obtained from conventional ANN, multivariate adaptive regression splines, and genetic programming, including the ANN optimized with particle swarm optimization developed in this study. Based on the experimental results of different settlement values, the newly constructed ANN-EO is very potential to analyze the risk associated with civil engineering structures. Also, the present study would significantly contribute to the knowledge pool of reliability studies related to piled raft systems because the works of literature on reliability analysis of piled raft systems are relatively scarce.

KEYWORDS

Risk analysis; soil; meta-heuristic optimization; particle swarm optimization

1 Introduction

Piled Raft Foundations (PRFs) have gained popularity among the engineering fraternity where it is necessary to transmit a large amount of superstructure load to the ground [1]. If normal pile foundations are adopted to carry a large incoming load, the depth of the piles becomes too large and it may prove to be uneconomical [2,3]. On the other hand, if only raft foundations are used,

the resultant settlements are usually too great which may impair the serviceability performance of the structure. In such a scenario, PRF may be chosen to carry the superstructure load where the combined presence of raft and piles will efficiently carry the incoming load and restrict the settlement within the permissible limits. Therefore, the installation of PRF allows an increase in the load capacity and reduction of settlements in a very economical way.

Griffith et al. [4] modeled rafts as a two-dimensional thin plate, in which the authors considered the piles a as one-dimensional rod element and soil as a vertical spring at each node. Later, this model was modified to take into account the effects of multilayered nonhomogeneous soil [5]. Poulos [6] modeled piles as interactive springs and soil as an elastic continuum. Brzakala et al. [7] performed the probabilistic analysis of raft foundations resting on layered subsoil. In the said study, the author performed a numerical analysis based on the finite element method coupled with stochastic versions of the perturbation and the Neumann expansion methods. Russo [8] modeled the piles as a nonlinear spring on the elastic continuum. Also, the idea of Winkler spring was successfully applied for modelling the piles as coupled spring [9]. Niandou et al. [3] developed a numerical model of a piled raft foundation to describe how the soil-structure interaction can be influenced by horizontal soil variability. Alkinani et al. [1] investigated the distribution of load under piled raft foundation considering the effect of piled raft geometry, length and diameter of piles, and other factors. Numerical analysis was employed by the authors to estimate the behavior of piled raft systems in soils under different conditions.

In this study, the settlement of a proposed PRF which supports a cantilever retaining wall is performed. The approach of Davis et al. [10] and Clancy et al. [11] was employed for this purpose. Note that, in geotechnical engineering practice, failure due to the settlement of foundations plays an important role. In general, the concept of factor of safety (FOS) is followed to estimate the settlement of foundations, which gives an approximate solution based on the deterministic values of basic soil parameters. Although, the FOS-based approach resulted in a conservative analysis; however, they turn out to be uneconomical in many cases [12]. In addition, it is common to use the obtained value of FOS for a given case, without regard to the degree of uncertainty involved in the calculation [13]. Hence, the FOS-based approach can be considered as irrational due to the fact that no information about geotechnical parameters (such as cohesion, angle of internal friction, bulk density, etc.) is complete, or even close to being complete, since soils display large variability in their properties [7].

Thus, to incorporate the uncertainties involved in solutions to geotechnical problems, careful consideration of geotechnical parameters should be ensured [7,13]. The reliability analysis (RA) seems to be a very useful numerical tool for this purpose. In general, RA provides a means of evaluating the effects of variability as well as uncertainties involved in geotechnical parameters [12]. It is pertinent to mention that, assessing the risk associated with the structures using reliability theory would require more data, time, and effort; however, following the concept of standard deviation and coefficient of variation [13], it is possible to make a useful evaluation of reliability. In this approach, the geotechnical parameters are treated as a random variable and the variation of these parameters are studied for the response of the concerned geotechnical structure. On the other hand, to lessen the time of performing the repeated task, soft computing techniques with their competence in non-linear modelling can be employed as an alternate tool based on the existing results of the problem under consideration [12,14,15]. Kumar et al. [12] used extreme learning machine (ELM) and multivariate adaptive regression splines (MARS) to perform RA of pile foundation. Kumar et al. [15] performed RA of the settlement of pile group using relevance vector machine (RVM), generalized regression neural network (GRNN), genetic programming

(GP), and adaptive-network-based fuzzy inference system (ANFIS). Kumar et al. [16] performed RA of pile foundation using minimax probability machine regression (MPMR), group method of data handling (GMDH), ANFIS, and emotional neural network (ENN). Kumar et al. [17] used RVM, MARS, and MPMR to determine the reliability index of cantilever retaining wall, Kumar et al. [18] used GP and MPMR for performing RA of circular footing, Roy et al. [19] used different soft computing techniques for shallow foundation reliability in geotechnical engineering.

In the field of engineering and sciences, the application of ANN has been highlighted by many researchers [20–24]. The greatest advantage of ANNs over other modeling techniques is the ability to model complex nonlinear processes without presuming a functional relationship between the input and output variables. However, ANN does present several limitations, such as its black-box nature, trapping into local minima, and overfitting related issues, etc. [25,26]. In addition, due to the weakness in finding the accurate global minimum, it may achieve undesirable results [24,27], especially in the validation phase. Therefore, to overcome these issues, several meta-heuristic optimization algorithms (OAs), such as particle swarm optimization (PSO), genetic algorithm (GA), grey wolf optimizer (GWO), imperialist competitive algorithm (ICA), artificial bee colony (ABC), biogeography-based optimization (BBO), salp swarm algorithm (SSA), gravitational search algorithm (GSA), etc., have been employed by the researchers, and hybrid models of ANN and OAs have been developed. Based on the powerful global search capabilities of these OAs, the learning parameters of ANN are optimized to enhance its performance prediction. In the past decade, several hybrid models such as ANN-PSO, ANN-GA, ANN-GWO, ANN-ICA, ANN-ABC, ANN-BBO, and so on, have been used extensively to solve nonlinear and complicated engineering problems [23,24,28–48].

In the present study, to perform the RA of a proposed PRF, a recently developed meta-heuristic OA called equilibrium optimizer (EO) has been used to optimize the learning parameters of ANN, and a hybrid model, i.e., ANN-EO is constructed. The reason behind the development of the ANN-EO model was to enhance the performance of the classical ANN algorithm. On the other hand, EO is a simple and efficient meta-heuristic OA, inspired by physics-based 'control volume mass balance' models. The authors of EO [49], suggested that EO is a significantly better algorithm and shows very competitive results compared to other well-established meta-heuristic OA, such as PSO, GA, GWO, SSA, and GSA. Elsheikh et al. [50] used EO to augment the prediction capability of random vector functional link network for predicting kerf quality indices during CO_2 laser cutting of polymethylmethacrylate, Foong et al. [51] used EO and vortex search algorithm for optimizing a multi-layer perceptron neural network to estimate the factor of safety of a single-layer soil slope, and Agnihotri et al. [52] used EO to solve economic dispatch problem having valve point effect, real power constraint, transmission line losses, ramp rate limits and prohibited zones of operation. Successful application of EO in different engineering disciplines can be found in the literature.

Taking these into consideration, EO was employed in the present study to enhance the performance of classical back-propagation ANN by optimizing the learning parameters of ANN. Furthermore, the outcome of the proposed ANN-EO model was compared with the other benchmark methods of classical back propagation ANN, GP, and MARS, including the PSO optimize ANN (ANN-PSO), another hybrid model proposed in this study. Subsequently, to perform the RA of PRF, an explicit relationship was considered, which gives the actual response of the structure as well as the implicit relationship between the input and output variables. However, prior to performing RA, the settlement of the proposed PRF was calculated. Subsequently, the reliability index (β) and probability of failure (POF) were calculated at different assumed values

of permissible settlement. To investigate the POF at different settlement values, a settlement range between 75 and 100 mm was considered and analyzed. In the present study, RA of a proposed retaining wall supported on piles is carried out. The wall supported on piles was modelled as per the theory of piled-raft foundation [53]. For this purpose, soil samples were collected during the geotechnical investigation process of the proposed conduction site of PRF located near the Harohar River, Lakhisarai, Bihar (India). 7 boreholes of 15 m each were dug and soil samples with the diameter of 38 mm were collected by the method of SPT. Necessary soil tests were carried out and the information related to geotechnical parameters was extracted and used in the present study to train and verify the proposed ANN-EO and ANN-PSO models.

The remainder of this study is organized as follows: Section 2 reviews the theoretical details of piled raft analysis, reliability analysis, and the details of employed soft computing models and meta-heuristic OAs. Section 3 describes the study site and the descriptive statistics of geotechnical parameters, while Section 4 presents the analysis of the proposed PRF. The next section, i.e., Section 5 reports the data processing and analysis, which is followed by the results, discussion, and conclusion in Sections 6–8, respectively.

2 Methodology

The following sub-sections describe the theoretical background of piled raft analysis. In this study, the PRF is designed following the earlier devised methods of Daviset al. [10] and Clancy et al. [11]. The methodology of RA is also discussed in the following sub-section.

2.1 Piled Raft Analysis

Davis et al. [10] and Clancy et al. [11] used several influencing factors to determine the settlement of the PRS which includes: correction factor for foundation flexibility; correction factors for Gibson soil profiles; displacement influence factor; and the correction factors for foundation embedment. Based on the type of foundation to be installed, the values of different corrections factors can be calculated as follows.

a) Correction factor for foundation flexibility: In reality, no structure is either fully rigid or fully flexible. Therefore, a correction factor (I_F) is introduced to consider the effect of the foundation rigidity which can be expressed as:

$$I_F \approx \frac{\pi}{4} + \frac{1}{4.6 + 10K_F} \tag{1}$$

where K_F is the foundation flexibility factor given by:

$$K_F \approx (E_{fdn}/E_{sAV})(t/a)^3 \tag{2}$$

where a is the equivalent radius of the foundation; E_{fdn} is the modulus of elasticity of foundation material; E_{sAV} represents equivalent modulus of elasticity of soil located beneath the foundation base; and t represents the thickness of the foundation. A foundation with different rigidity conditions, the values of K_F are given by:

- For a perfectly rigid foundation, $K_F > 10$.
- Foundation with intermediate flexibility, $0.01 \leq K_F \leq 10$.
- For a perfectly flexible foundation, $K_F < 0.01$.

b) Correction factor for Gibson soil profiles: A soil whose modulus of elasticity (E_S) increases linearly w.r.t. the depth is termed as Gibson soil. The behavior of Gibson soil can be expressed as follows:

$$E_S = E_0 + k_E z \tag{3}$$

where E_0 is the modulus of elasticity of soil below the foundation and k_E is the rate of increase of modulus of elasticity with depth is known as correction factors for Gibson soils.

c) Displacement influence factor: The expression for calculating displacement influence factor is given by:

$$I_G \approx \frac{1}{1 + 0.6\beta_G{}^{-0.8}} \tag{4}$$

where β_G is termed as normalized Gibson modulus ratio whose value generally lies in the range of 0.01 to 100. The expression for calculating β_G is given by:

$$\beta_G = E_0/(k_E.d) \tag{5}$$

d) Correction factor for foundation embedment: The correction factor for embedment of foundation base (I_E) suggested by Burland [54] is the function of the proportion of embedment depth (z_E) to the foundation diameter (d) and Poisson's ratio (ν) of the supporting soil medium, is given by:

$$I_E \approx 1 - \frac{1}{3.5\exp(1.22\nu - 0.4)[(d/z_E) + 1.6]} \tag{6}$$

Considering all the correction factors, the final expression for calculating the settlement at the center of shallow spread footings and mat foundations can be given as:

$$\rho_{center} = \frac{qdI_F I_G I_E(1-\nu^2)}{E_0} \tag{7}$$

where I_F, I_G and I_E are the corresponding correction factor given in Eqs. (1), (4), and (6), respectively. In addition to the correction factors, the stiffness of raft foundation and stiffness of pile group can be calculated as follows:

i. Stiffness of raft foundation

The ratio of the load and its corresponding settlement at the center of the raft is known as the stiffness of the raft foundation and is denoted by K_r. The expression of which is given by:

$$K_r = \frac{\text{Load on raft}}{\text{Settlement at the center of raft}} = \frac{P_r}{\rho_{center}} = \frac{(\pi/2)d_{raft}G_0}{I_G I_F I_E(1-\nu_{soil})} \tag{8}$$

where d_{raft} is the equivalent raft diameter.

ii. Stiffness of pile group

To determine the stiffness of the pile group, the stiffness of the single pile should be determined first. Using the concept of group efficiency of piles proposed by Fleming et al. [55], the

stiffness of the combined piled group can be estimated. The single pile head response is given by the formula suggested by Randolph et al. [53] using the linear load transfer function, given by:

$$\frac{P_t}{Glr_0w_t} = \frac{\frac{4\eta}{(1-\nu)\xi} + \rho\frac{2\pi}{\zeta}\frac{\tanh\mu l}{\mu l}\frac{l}{r_0}}{1 + \frac{1}{\pi\lambda}\frac{4\eta}{(1-\nu)\xi}\frac{\tan\mu l}{\mu l}\frac{l}{r_0}} \tag{9}$$

where P_t and w_t are the total load and displacement at the top of the pile, respectively; G is the value of modulus of shear at a depth of z; l and r_0 are the length and radius of the pile, respectively. Some other parameters useful for modeling PRS are given below:

- For Under-reamed pile: $\eta = \frac{r_b}{r_0}$; for end-bearing pile: $\xi = \frac{G_l}{G_b}$; herein, the subscript b refers to any parameter at or below the base of the pile.
- ρ is a heterogeneity factor for soil modulus which is expressed as: $\rho = \frac{G_{avg}}{G_l}$.
- The soil-pile stiffness ratio λ is expressed as: $\lambda = \frac{E_p}{G_l}$.
- ζ is the ratio of maximum radius of influence (r_m) and radius of pile (r_0), given by: $\zeta = \ln(r_m/r_0)$.
- Maximum radius of influence (r_m) can be calculated using the following expressions:

$$r_m = [0.25 + \xi\{2.5\rho(1-\nu) - 0.25\}] \quad l \text{ for } \xi \neq 1 \tag{10}$$

and, in case of friction pile, it is given by:

$$r_m = 2.5\rho(1-\nu) \quad l \text{ when } \xi = 1 \tag{11}$$

- The effect of compressibility of pile (μl) is given by: $\mu l = \sqrt{2/\zeta\lambda}(l/r_0)$.
- The proportion of load reaching the pile base is given by:

$$\frac{P_b}{P_t} = \frac{\frac{4\eta}{(1-\nu)\xi}\frac{1}{\cosh\mu l}}{\frac{4\eta}{(1-\nu)\xi} + \rho\frac{2\pi}{\zeta}\frac{\tan\mu l}{\mu l}\frac{l}{r_0}} \tag{12}$$

- From the equations stated above, the single pile stiffness is evaluated as follows:

$$\frac{P_t}{w_t} = k_1 = G_l r_0 \frac{\frac{4\eta}{(1-\nu)\xi} + \rho\frac{2\pi}{\zeta}\frac{\tanh\mu l}{\mu l}\frac{l}{r_0}}{1 + \frac{1}{\pi\lambda}\frac{4\eta}{(1-\nu)\xi}\frac{\tanh\mu l}{\mu l}\frac{l}{r_0}} \tag{13}$$

Due to interaction effects, the stiffness of each pile in a group is reduced in comparison to a single pile. This may be quantified using efficiency factor η as given below:

$$\eta \approx n^{-e} \tag{14}$$

where n represents the number of piles in the pile group. The group stiffness (k_p) is expressed as:

$$k_p \approx n^{1-e}k_1 \tag{15}$$

where n is the total number of piles in a pile group; k_1 is the stiffness of a single pile; e is the exponent correction factor which generally lies in the range of 0.3 to 0.5 for primarily friction piles, rising to 0.6 or higher for end-bearing piles. For friction piles, Randolph et al. [53] and proposed a set of design charts which is generally used to obtain the values of e. The exponent

term is expressed in terms of a base value e_1 as a function of the slenderness ratio $\left(\frac{l}{d}\right)$ of the pile and four characteristics factors c_1, c_2, c_3 and c_4 [55]. The characteristic factors are the functions of stiffness ratio $\left(\frac{E_p}{G_1}\right)$, spacing ratio $\left(\frac{s}{d}\right)$, homogeneity factor (ρ) and Poisson's ratio (ν). The term e is expressed as follows:

$$e = e_1(l/d) \times c_1(E_p/G) \times c_2(s/d) \times c_3(\rho) \times c_4(\nu) \tag{16}$$

iii. Interaction factors

Interaction factor α, which is used to consider the effect of adjacent piles in the pile group. It is expressed as the ratio of additional settlement contributed by the adjacent piles to the settlement caused due to a single pile. A pile with a circular cap of radius r_c (refer Fig. 1a), the expression for interaction factor can be given by [54]:

$$\alpha_{rp} = 1 - \frac{\ln(\frac{r_c}{r_0})}{\zeta} \tag{17}$$

where r_c represents the average radius of pile cap; r_0 is the radius of pile; and $\zeta = ln\frac{r_m}{r_0}$. Herein, the term r_m can be calculated using the following expression:

$$r_m = [0.25 + \xi\{2.5\rho(1 - \nu_s) - 0.25\}]l \tag{18}$$

where $\xi = \frac{G_l}{G_b}$; $\rho = \frac{G_{avg}}{G_l}$; $\nu_s =$ Poisson's ratio of soil; and $l =$ pile length. The expression given in Eq. (17) may also be used for larger pile groups. $E_{sl} =$ equivalent modulus of elasticity of soil at the level of pile tip; E_{sb} is the equivalent modulus of elasticity of soil at bearing stratum below pile tip; and E_{sAV} is the average equivalent modulus of elasticity of soil along pile shaft. The graphical representation of modulus of elasticity with respect to depth for a simplified pile cap unit is shown in Fig. 1b. Poulos et al. [56] proposed a relationship for calculating combined piled-raft stiffness K_{pr} as follows:

$$K_{pr} = \frac{K_p + K_r(1 - 2\alpha_{cp})}{(1 - \alpha_{cp}{}^2 K_r/K_p)} \tag{19}$$

where K_p is the stiffness of the pile group; K_r is the stiffness of raft; and α_{cp} is the raft-pile interaction factor.

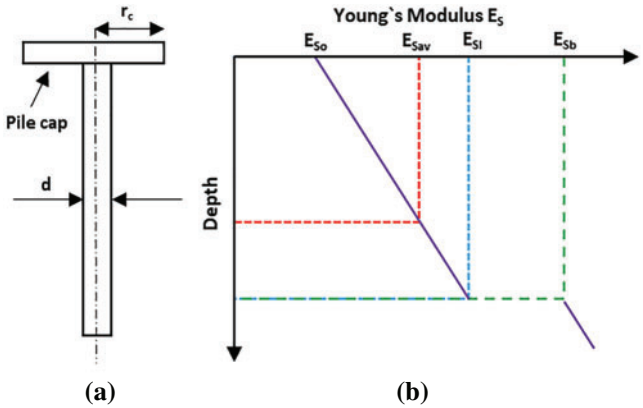

Figure 1: (a) Pile profile and (b) representation of modulus of elasticity of a simplified piled raft unit

The raft stiffness can be calculated using the formula given by Mayne et al. [57]. Also, single pile stiffness is calculated from the elastic theory and then multiplied by a group stiffness efficiency factor, which is estimated approximately from elastic solutions as discussed before. The proportion of the total applied load carried by the raft is:

$$\chi = \frac{Pr}{Pt\frac{K_r(1-\alpha_{rp})}{K_p+K_r(1-\alpha_{cp})}} \tag{20}$$

where $P_r =$ Load carried by the raft; $P_t =$ Total applied load. Therefore, the total load is shared between the raft and the pile group in proportion to weightage factors χ and $(1-\chi)$, respectively. If P_1 be the total incoming load on the PRF and P_{up} be the pile group capacity, then the total applied load P_1 at which the pile capacity reached is expressed in Eq. (21) as per [10]:

$$P_1 = \frac{P_{up}}{1-\chi} \tag{21}$$

The individual pile capacity for the present work is determined as per IS 2911 (Part 1: Section 2): 2010. The group capacity P_{up} is later obtained by multiplying the individual pile capacity with the total number of piles present in the pile group.

2.2 Calculation of Settlement

Davis et al. [10] proposed a simplified load versus settlement curve to estimate the settlement of PRF (refer Fig. 2), the first part of this curve (from point **O** to point **A**) is used when the total applied load (P_1) is less than the load at which pile group capacity (P_{up}) is reached, i.e., $P_1 < P_{up}$; Up to this point (point **A**) both pile and raft remain elastic. In this case, the settlement of raft can be expressed as the ratio of total externally applied load to the stiffness of PRF, given by:

$$\text{for } \mathrm{P_1 < P_{up}}, \quad S_{pr} = \frac{P_{up}}{K_{rp}} \tag{22}$$

On the other hand, when the total applied load (P_1) exceeds the pile group capacity, i.e., $P_1 > P_{up}$; the settlement of PRF can be calculated using the expression given below:

$$\text{for } \mathrm{P_1 > P_{up}}, \quad S_{pr} = \frac{P_1}{K_{rp}} + \frac{P-P_1}{K_r} \tag{23}$$

2.3 Reliability Analysis (RA)

The reliability of a geotechnical structure is its ability to fulfill its design objectives for a given period under certain loading conditions. In other words, it is the probability that the structure does not reach the specified limit state for a specified period. For carrying out RA, it is necessary to define relationships between a set of input and output variables. Explicit relationship for RA was obtained from the analytical formulation given by Davis et al. [10] and Clancy et al. [11]. In the present work, the reliability of the PRF was performed based on serviceability limit state

criterion; and the method adopted for RA is the First Order Reliability Method (FORM). A brief description of the said method is described below.

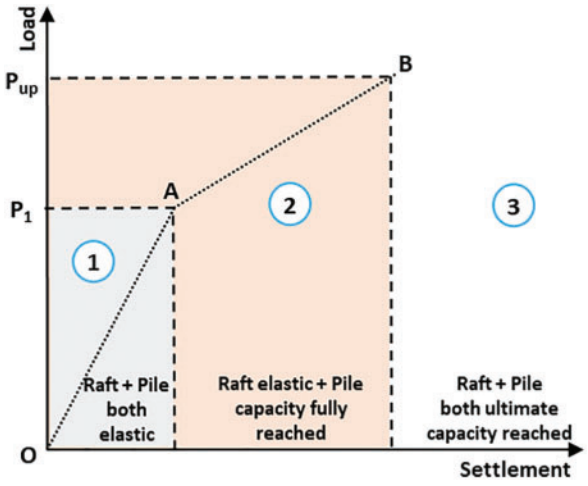

Figure 2: Load settlement curve for a simple PRF [10]

FORM is based upon the first few terms of Taylor's series expansion [58]. This method is useful for estimating the mean value and variance of the performance function. FORM is often referred to as the first-order second-order method (FOSM).

Let the demand (expected loadings) of an engineering system is D_L and the capacity (available resistance) is C_R. Note that, generally, the values of both C_R and D_L are uncertain. The associated variables have mean or expected values, variances and covariance. The margin of safety of the system is expressed as a limit state function often known as performance function (C_R, D_L) . Hence, the failure surface equation can be described as follows:

$$M = C_R - D_L = 0. \tag{24}$$

This limit state function divides a region between the safe and unsafe condition. The probability of failure may be expressed as:

$$p_f = P[(C_R - D_L) \leq 0] \tag{25}$$

Using the above equations, the reliability index, β can be calculated using the expression given below:

$$\beta = \frac{\mu_C - \mu_D}{\sqrt{(\sigma_c{}^2 + \sigma_D{}^2)}} \tag{26}$$

where μ_C and μ_D are the mean of capacity and demand, respectively; σ_C and σ_D are the corresponding standard deviations of capacity and demand. The probability of failure is given by;

$$p_f = 1 - \phi\left[\frac{\mu_C - \mu_D}{\sqrt{(\sigma_c{}^2 + \sigma_D{}^2)}}\right] \tag{27}$$

where $\phi(..)$ is the cumulative distribution function for the standard normal variate. More details of this technique can be found in the literature [14,15,59–62]. A process diagram of RA is presented in presented in Fig. 3, in which both actual and computational process of calculating POF are presented.

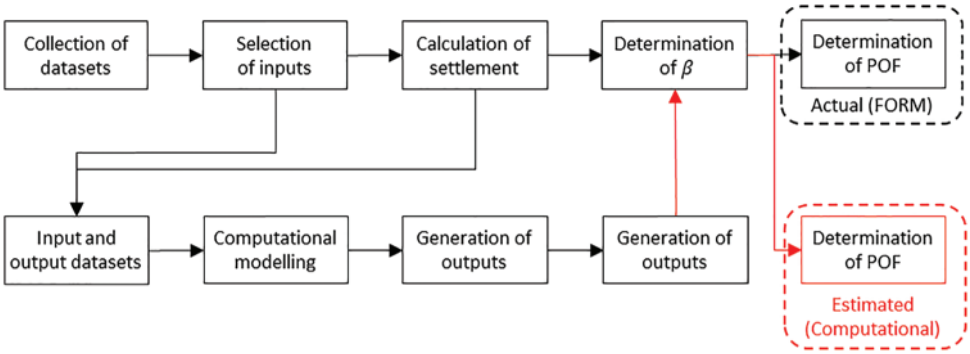

Figure 3: A process diagram of RA through FORM and computational modelling

2.4 Theoretical Background of the Employed Algorithms

In this sub-section, short descriptions of different soft computing techniques are presented. Begin with presenting the methodologies of ANN, GP, and MARS used in this study, which is followed by discussing the working principle of EO and PSO. Finally, the hybridization process of ANN-based hybrid models, i.e., ANN-EO and ANN-PSO are presented.

2.4.1 Artificial Neural Network (ANN)

ANN is a bio-inspired computing model made up of hundreds of individual units (artificial neurons) attached to coefficients (weights) that establish the neural structure. A structure of ANN consists of an input layer, hidden layer, and output layer with one or more neurons in each layer. As they play a role in information processing, they are also called processing elements (PEs). Each PE has its output, weighted inputs, and transfer function. PE is basically an equation that strikes a balance between inputs and outputs. Since connection weights denote the system memory, ANNs are also referred to as connectionist models. ANN has become a popular mathematical instrument for various purposes, including function approximation and pattern recognition. Successful application of this ML algorithm can be found in the literature [22–24,26,27].

2.4.2 Genetic Programming (GP)

GP is a symbolic optimization technique that creates computer programs based on the principle of Darwinian natural selection [63–65]. It is an extension of genetic algorithms (GA). The method was originally proposed by Koza [66], which mimics the biological evolution of living organisms. In GP, initially, a random population of individuals is created to achieve high diversity. Note that, the creation of initial populations is a blind random search. Once the initial population is created, GP evaluates individuals, selects them for reproduction, and generates new individuals by mutation, crossover, and reproduction; and finally, it creates new generations in all iterations.

In GP, the evolutionary process (a combination of crossover, mutation, and reproduction) continues by evaluating the fitness of the new population and starts a new round of evolutionary process in the next iteration. The best program that appeared in any generation, the best-so-far

solution, defines the output of the GP algorithm. Successful implementation of this regression technique can be found in the analysis of slope stability, liquefaction susceptibility, compressive strength of concrete, including other areas of civil engineering [63–65,67–75].

2.4.3 Multivariate Adaptive Regression Splines (MARS)

MARS, introduced by Friedman [76] is a non-parametric regression technique that is capable of modelling non-linear relationships between the independent and dependent variables. It uses series of piecewise linear segments having different gradients known as splines. Splines are the flexible linear lines that are linked with knots. MARS simplifies complex multivariate datasets to relatively simple and linear additive models. It uses recursive partitioning and spline fitting to handle both quantitative and categorical predictors.

In the first phase, i.e., forward phase, it selects only one input variable and placed the knots at random positions within the range of each predictor to define a pair of Basis functions (BFs). BFs is nothing but a spline. In each step, the knot and its corresponding pair of BFs are fitted to yield the maximum reduction in sum-of-squares residual error by adding new BFs until the minimum threshold value is reached. However, the addition of BFs yields a complex and over-fitted model which shows poor performance for the new dataset.

In order to improve the performance of the over-fitted model, MARS starts pruning of least performing BFs in the subsequent phase, i.e., deletion of BFs takes place in the phase. Generally, MARS removes one BF at a time and assesses the model based on the generalized-cross-validation (GCV) criterion [72,77]. This process continues until the lack-of-fit criterion is minimum. Finally, produced the optimum model with the optimum number of BFs.

2.4.4 Equilibrium Optimizer (EO)

EO is a recently developed meta-heuristic optimization algorithm [49], resourced from physics-based dynamic mass balance theory. It typically characterizes the interaction of search agents according to governing rules rooted in physical processes. The working principle of EO is similar to the other metaheuristics algorithms where the search operation is performed using a set of candidate solutions. During the search, the candidate solutions update their concentration with respect to the best solution obtained till that point, to finally arrive at the equilibrium state, which provides the optimal result. These candidate solutions are called concentration vectors (CVs) given by:

$$C_i = C^{min} + rand \times \left(C^{max} - C^{min}\right), \quad i = 1, 2, \ldots, N \tag{28}$$

where C_i is the i^{th} CVs; $C^{max}$and C^{min} are the upper and lower bound vectors; the function/term *rand* indicates random numbers between 0 and 1 (uniformly distributed); and N is the number of particles. In each iteration, particles are evaluated based on their fitness function and sorted to determine the equilibrium candidates. The mathematical expression used to update the CVs can be given by:

$$C_i^{t+1} = C_{EQ}^t + \left(C_i^t - C_{EQ}^t\right) \times F_i^t + \left(1 - F_i^t\right) \times \frac{G_i^t}{\lambda_i^t V_i^t} \tag{29}$$

where C_{EQ}^t is the equilibrium concentration; C_i^t and C_i^{t+1} are the CVs in t and $t+1$ iterations, respectively; the term $\left(C_i^t - C_{EQ}^t\right) \times F_i^t$ is responsible for global search in the exploration stage,

and the final term $\left(1-F_i^t\right)\times\frac{G_i^t}{\lambda_i^t V_i^t}$ is responsible for the exploitation operation. It also extracts useful information from the explored search area. The randomly selected CVs, i.e., C_{EQ}^t, from the equilibrium pool can be constructed as follows:

$$C_{EQ}^t=\left\{C_{EQ_1}^t,C_{EQ_2}^t,C_{EQ_3}^t,C_{EQ_4}^t\right\} \tag{30}$$

where $C_{EQ_1}^t,C_{EQ_2}^t,C_{EQ_3}^t$, and $C_{EQ_4}^t$, are the first four best CVs considered as approximated equilibrium states. In EO, the exponential term F_i^t given in Eq. (31), which controls the exploration and exploitation operation during the search.

$$F_i^t=exp\left(\left(T-T_0\right)\lambda_i^t\right) \tag{31}$$

$$T=\left(1-\frac{t}{t_{max}}\right)^{a_2\times t/t_{max}} \tag{32}$$

$$T_0=T+\frac{1}{\lambda_i^t}\times ln\left(-a_1 sign(r-0.5)(1-e^{\lambda T})\right) \tag{33}$$

where t and t_{max} denote the current iteration and the maximum number of iterations, respectively; a_1 is the exploration controlling parameter; r is a random number uniformly distributed between 0 and 1. The values of a_1 and a_2 are fixed to 2 and 1, respectively; the term $sign(r-0.5)$ is used to decide the direction of exploration and exploitation operation. Substituting the term of Eqs. (32) and (33) in Eq. (31), the final expression of F_i^t can be given by:

$$F_i^t=a_1\times sign(r-0.5)(e^{-\lambda_i^t T}-1) \tag{34}$$

The iteration rate G_i^t contributes in exploiting the search space during the process of search, which are given by:

$$G_i^t=G_0^t\times exp\left(\left(T-T_0\right)\times\lambda_i^t\right) \tag{35}$$

$$G_0^t=p_i^t\times\left(C_{EQ}^t-\lambda_i^t C_i^t\right) \tag{36}$$

$$p_i^t=\begin{cases}0.5 & r_1 r_2\geq g_p^t\\ 0 & otherwise\end{cases} \tag{37}$$

where p_i^t denotes the iteration rate; g_p^t is the iteration probability; and r_1 and r_2 are the two random numbers, which are uniformly distributed between 0 and 1.

2.4.5 Particle Swarm Optimization (PSO)

PSO is a population-based meta-heuristic algorithm introduced by Kennedy et al. [78] as a member of the swarm-based community. The PSO algorithm has mainly been inspired by fish schools or bird flocks, whose main purpose is to find globally optimal solutions in a multidimensional space. It starts with the initialization of particle positions and random velocities. To find the best position in the multidimensional space, each particle then attempts to update its position based on its velocity, as well as the personal best position (best position reached by a single particle) and global best position (best position reached by individual particles). The position of each particle is updated based on its personal best position and the direction of the global best

position. Meanwhile, particle velocity is updated according to the difference between its personal and global best positions. The particles then use a combination of exploration and exploitation to converge around the optimal solution. The velocity and position of a particle in each iteration is given by:

$$V_i^{t+1} = \omega V_i^t + c_1 r_1^t \left(P_i^t - X_i^t\right) + c_2 r_2^t (P_g^t - X_i^t) \tag{38}$$

$$X_i^{t+1} = X_i^t + V_i^{t+1} \tag{39}$$

where P, V, g, and i stand for position, velocity, global, and personal, respectively; r_1 and r_2 are two random numbers in the range [0, 1]; c_1 and c_1 are the acceleration parameters demonstrating a particle's confidence level against its personal position and global position; and ω is the inertia weight. The decreasing trend of inertia weight over time is shown below:

$$\omega^t = \omega_{max} - \frac{\omega_{max} - \omega_{min}}{t_{max}} t \tag{40}$$

where ω_{min} and ω_{max} denote primary inertia weight and final inertia weight, respectively; t_{max} is the maximum number of iterations. PSO is quite similar to GA, except that in the former, particles support each other, and in the latter, they compete with each other. PSO is distinguished from other optimization methods by its large particle number, enabling us to find globally optimal solutions.

2.4.6 Hybridization of ANN-Based Meta-Heuristic Models

In engineering applications, many studies have been performed to enhance the performance of traditional ML algorithms by implementing meta-heuristic OAs, such as PSO, GA, etc. Due to the weakness of traditional ML algorithms, such as ANN, in finding the exact global minimum, ANN may produce undesirable results [24,27]. In addition, ANN is more likely to be caught up in local minima. Therefore, implementing meta-heuristic OAs can solve the problem by optimizing the learning parameters (weights and biases) based on error criteria.

In this study, two meta-heuristic OAs, namely EO and PSO are used to optimize the weights and biases of conventional ANN. The learning parameters of ANN include input to hidden weights, hidden biases, hidden to output weights, and output biases. A model with i input(s), h hidden neuron(s) and o output(s), the total number of weights and biases will be $i \times h + h + h \times o + o$. The methodical development of the ANN coupled EO (ANN-EO) and ANN coupled PSO (ANN-PSO) can be described as follows: a) selection of hyper-parameters (number of hidden neurons and activation function) of ANN; b) random generation of weight and biases; c) selection of different parameters of meta-heuristic OAs, such as maximum number of iteration, population/particle size, upper and lower bounds, etc.; d) training of ANN through OAs; e) generation of optimized values of weight and biases; f) check error criteria and maximum number of iteration; and g) selection of optimal values of optimized weight and biases based on minimum error criteria. Finally, the optimized learning parameters were used to predict the new dataset, i.e., the testing dataset. Note that, although the procedure for developing the ANN-EO and ANN-PSO are the same; however, the values of optimized weight and biases are different for the said models. A flow chart showing the steps of ANN-based hybrid modeling is shown in Fig. 4.

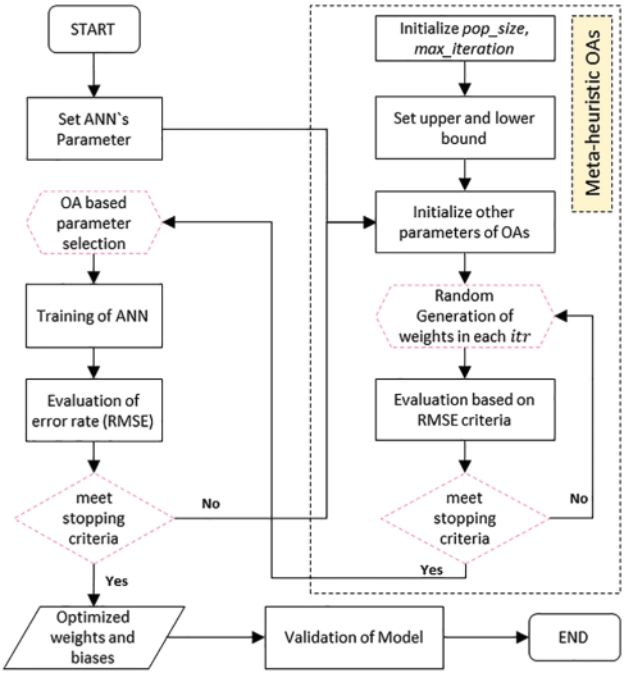

Figure 4: Flow chart showing the steps in developing ANN-based hybrid models

2.4.7 Performance Evaluation

To assess the performance of the developed models, six widely used performance indices, namely determination coefficient (R^2), Willmott's Index of agreement (WI), Legates & McCabe's Index (LMI), root mean square error (RMSE), mean absolute error (MAE), and weighted mean absolute error (WMAPE) were determined and assessed in detail. The details of these indices can be found in the literature [16,79–86]; however, for convenience, the mathematical expressions are given below. In addition, for a perfect predictive model, the ideal values of these indices are given in Tab. 1.

$$R^2 = \frac{\sum_{i=1}^{n}(y_i - y_{mean})^2 - \sum_{i=1}^{n}(y_i - \hat{y}_i)^2}{\sum_{i=1}^{n}(y_i - y_{mean})^2} \tag{41}$$

$$WI = 1 - \left[\frac{\sum_{i=1}^{n}(y_i - \hat{y}_i)^2}{\sum_{i=1}^{n}\left\{\left|\hat{y}_i - y_{mean}\right| + \left|y_i - y_{mean}\right|\right\}^2}\right] \tag{42}$$

$$LMI = 1 - \left[\frac{\sum_{i=1}^{n}|y_i - \hat{y}_i|}{\sum_{i=1}^{n}|y_i - y_{mean}|}\right] \tag{43}$$

$$RMSE = \sqrt{\frac{1}{n}\sum_{i=1}^{n}(y_i - \hat{y}_i)^2} \tag{44}$$

$$MAE = \frac{1}{n}\sum_{i=1}^{n}\left|(\hat{y}_i - y_i)\right| \tag{45}$$

$$WMAPE = \frac{\sum_{i=1}^{n} \left| \frac{y_i - \hat{y}_i}{y_i} \right| \times y_i}{\sum_{i=1}^{n} y_i} \tag{46}$$

where y_i represents the measured value; $\hat{y}_i$ represents the predicted value; y_{mean} is the mean of the measured variables; and n is the total number of observations under consideration. Among these indices, R^2, WI, and LMI measure the linear regression relationship between the measured and predicted variable, whereas RMSE, MAE, and WMAPE determine the error associated with the prediction models.

Table 1: Ideal values of different performance indices

Particulars	Performance parameters					
Parameter	R^2	WI	LMI	RMSE	MAE	WMAPE
Ideal value	1	1	1	0	0	0

3 Description of the Study Site and Collected Dataset

The site under consideration is located near the Harohar River (lat. 25° 12′49.5″ N, long. 86° 04′13.9″ E) was selected as the study area. A 2.5 m wide approach road was planned to be built towards a bridge over the river Harohar. Since the proposed level of the approach road was higher than the existing ground level aligning with the river; the soil was dumped to raise the existing ground level up to the level of the approach road. But, after filling of soil material, bearing capacity failure was observed for the existing ground level. Later, a cantilever retaining wall was proposed to be constructed at the site in order to support the soil standing up to the level of the approach road. The details of the cantilever retaining wall are shown in Fig. 5. It is observed that the underlying soil has poor properties in terms of cohesion (C) and angle of internal friction (ϕ). Therefore, to safeguard against possible failure of the structure due to poor soil properties, the base slab was planned to be supported on piles extending up to a depth of 15 m or at least where the sand layer was found. In the present work, the base slab along with piles are modeled as per the theory of PRF proposed by Clancy et al. [11], and the resulting settlement of the whole system was calculated accordingly.

To obtain information about the sub-soil conditions, 7 boreholes of 15 m each were dug and soil samples with a diameter of 38 mm were collected by the method of SPT. The soil samples were collected at an interval of 1.5 m depth. After the geotechnical investigation, necessary soil tests were carried out and the information extracted from the tests include C, ϕ, and bulk density of soil (γ). These soil parameters along with Young's modulus of soil (E_{soil}), Young's modulus of pile material (E_{conc}), Poisson ratio of soil (ν_{soil}), Poisson ratio of pile material (ν_{conc}), and adhesion factor of pile and soil (α) were considered for the settlement calculation of PRF. These parameters are the most influencing factors and hence were used as input parameters to estimate the settlement of PRF. Tab. 2 represents the minimum and maximum values of the input parameters obtained from soil investigation reports.

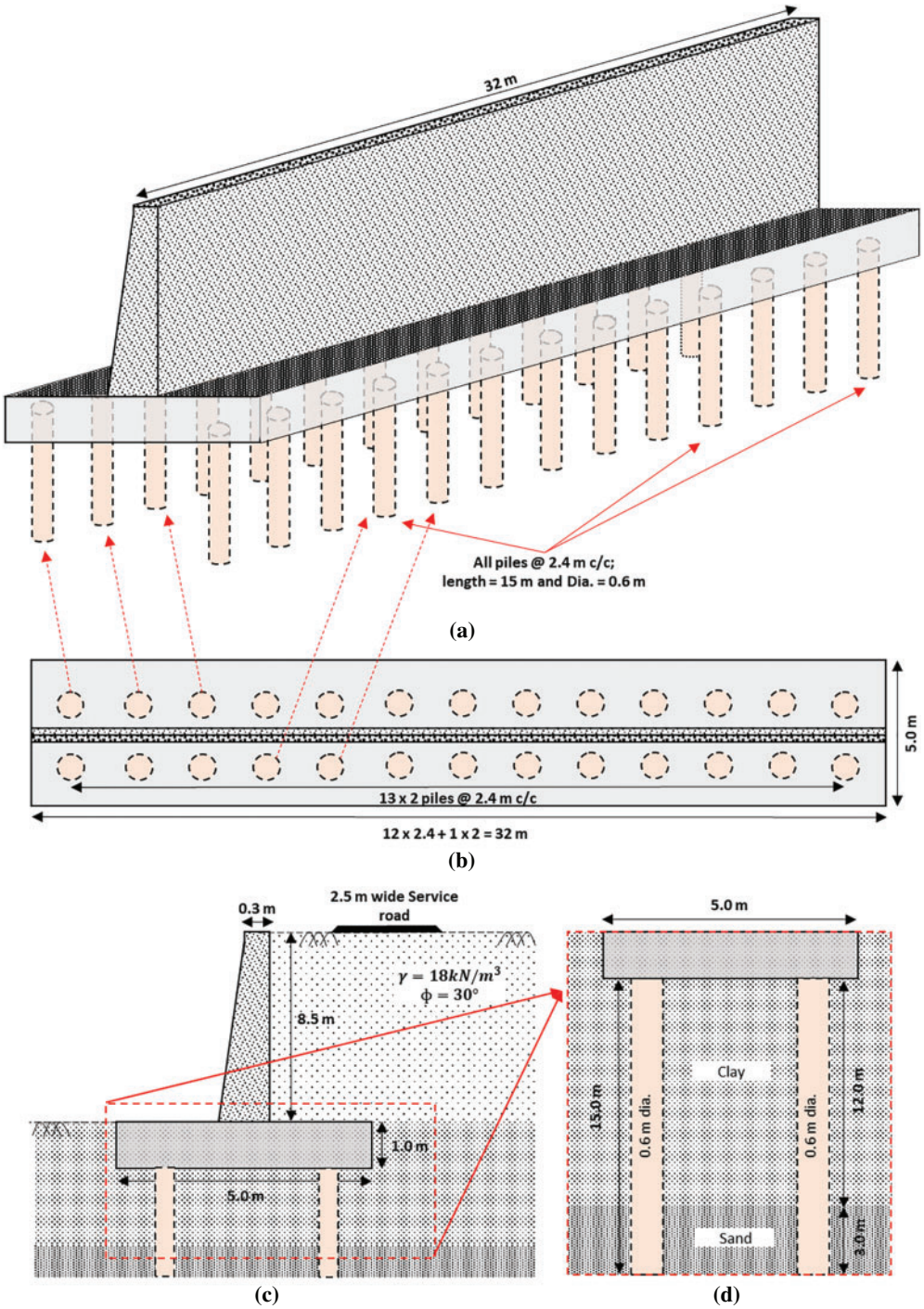

Figure 5: Schematic details of the proposed PRS: (a) Cantilever retaining wall with pile arrangement; (b) top view of PRS; and (c, d) sectional view of PRS

Table 2: Details of soil properties and pile material

Input parameters		Unit	Min. value	Max. value
C	Cohesion	kN/m^2	21.02	29.93
ϕ	Angle of internal friction	°	27.33	35.89
γ	Bulk density of soil	kN/m^3	14.02	16.99
E_{soil}	Young's modulus of soil	N/mm^2	9.20	75.41
E_{conc}	Young's modulus of pile material	N/mm^2	20022	29969
ν_{soil}	Poisson ratio of soil	–	0.25	0.40
ν_{conc}	Poisson ratio of pile material	–	0.20	0.35
α	Adhesion factor of pile and soil	–	0.70	0.99

4 Analysis of Proposed PRF

In this section, the analysis of the proposed PRF, which is supposed to carry the load from a cantilever retaining wall is presented. Fig. 5 shows the details of PRF, including the details of each pile and sub-soil properties. As can be seen, the proposed PRF consists of 26 piles, a 1 m thick raft, and an 8.5 m high cantilever retaining wall with a 5 m wide base. All piles are 15 m long and 0.6 m in diameter. The spacing between the piles is 2.4 m in both directions. The overall height of the retaining wall including the raft is 9.5 m. The width of the stem of the retaining wall at the top is 0.30 m, and it increased to 0.6 m at the base giving a clearance of 2.2 m on each side of the raft. The cantilever retaining wall was designed to construct the approach road as shown in Fig. 5c.

Different soil properties, such as C, ϕ, and γ, including the standard penetration test (SPT) value, i.e., N value were collected from the project site. Seven boreholes were dug to carry out the soil investigation work. Based on the bore-log and soil test report, it was observed that the first 12 m soils were clayey in nature and below 12 m depth, it was mainly sandy soil. The soil which was dumped to raise the level of the existing ground level to the level of the approach road was mainly sandy soil with $\gamma = 18$ kN/m^3 and $\phi = 30°$.

In the first step, the incoming load and the moment on the PRF were calculated. The retaining wall is shown in Fig. 5c, was analyzed for the total height of the backfill material with soil properties $\gamma = 18$ kN/m^3, $\phi = 30°$, and $\nu_s = 0.50$. Using the expressions (19), (22) and (23) given in the methodology section, the stiffness of the pile group and its corresponding settlement were calculated as 1.805 MN/mm and 66.08 mm, respectively.

In the subsequent step, RA of PRF was performed considering the most important influencing parameters, i.e., C, ϕ, γ, E_{soil}, E_{conc}, ν_{soil}, ν_{conc}, and α. The parameters C, ϕ, γ, and E_{soil} considered in the analysis are C_{avg} (average cohesion for the 12 m clay layer), ϕ_{avg} (average angle of internal friction for the 3 m sand layer), ϕ_b (angle of internal friction at the pile bottom), γ_{avg} (average bulk density of soil for the layer under consideration), E_{S0} (Young's modulus of soil at the pile top), E_{Sm} (Young's modulus of soil at the mid-depth) and E_{Sb} (Young's modulus of soil at the pile bottom). To perform the RA, 80 random datasets were generated considering the maximum and minimum values of soil properties (refer Tab. 2), obtained from the soil test reports, and the settlement of PRS was calculated for each dataset. Subsequently, β and POF of PRF were calculated. Descriptive statistics and scatter density plots of the variables are shown in Tab. 3 and Fig. 6, respectively.

It is pertinent to mention here that, the aforementioned parameters (C, ϕ, γ, E_{soil}, E_{conc}, ν_{soil}, ν_{conc}, and α) are mainly cohesion, angle of internal friction, bulk density, young's modulus, and Poisson ratio of soil along with Poisson ratio of pile material, and are important properties of soil and pile materials. These parameters were used to calculate the settlement of PRF. Therefore, these parameters are responsible for pile settlement and are considered in the present analysis as the input parameters.

Table 3: Descriptive statistics of the input and output variables

Parameters	Unit	Min.	Avg.	Max.	Stnd. error	Stnd. Dev.	Kurtosis	Skewness
γ_{avg}	kN/m^3	14.02	15.59	16.99	0.1	0.9	−1.26	−0.07
E_{S0}	N/mm^2	9.2	17.6	25.1	0.62	5.59	−1.43	−0.19
E_{Sm}	N/mm^2	18.4	35.2	50.2	1.25	11.17	−1.43	−0.19
E_{Sb}	N/mm^2	54.97	63.12	75.41	0.59	5.27	−0.48	0.49
E_{conc}	N/mm^2	20022	25403	29969	326	2913	−1.23	−0.18
C_{avg}	kN/m^2	21.02	25.46	29.93	0.31	2.73	−1.29	−0.01
ϕ_{avg}	°	28.04	32.22	35.89	0.25	2.21	−1.11	−0.12
ϕ_b	°	27.33	31.47	35.69	0.29	2.55	−1.25	0.15
α	–	0.7	0.85	0.99	0.01	0.09	−1.21	−0.13
ν_{soil}	–	0.25	0.34	0.4	0	0.04	−1.1	−0.36
ν_{conc}	–	0.2	0.28	0.35	0	0.04	−1.37	−0.11
Settlement	mm	41.79	57.54	76.28	1.01	9.02	−0.8	0.42

5 Data Processing and Analysis

The most crucial step for any type of problem in the field of soft computing techniques, such as ANN techniques, is considered to be the normalization of data. This is a pre-processing phase. In the present study, 80% of the total dataset, i.e., the training dataset was used to construct the models, while the balance 20% dataset (testing dataset) was used to validate the developed models. Before the training and testing bifurcation, the total dataset was normalized in the range of 0 to 1 using the expression given by:

$$x_{norm} = \frac{x_i - x_{min}}{x_{max} - x_{min}} \tag{47}$$

where x_i is the i^{th} instance of the dataset under consideration, x_{norm} is the normalized values of x_i, x_{min} and x_{max} represent the minimum and maximum values of x_i.

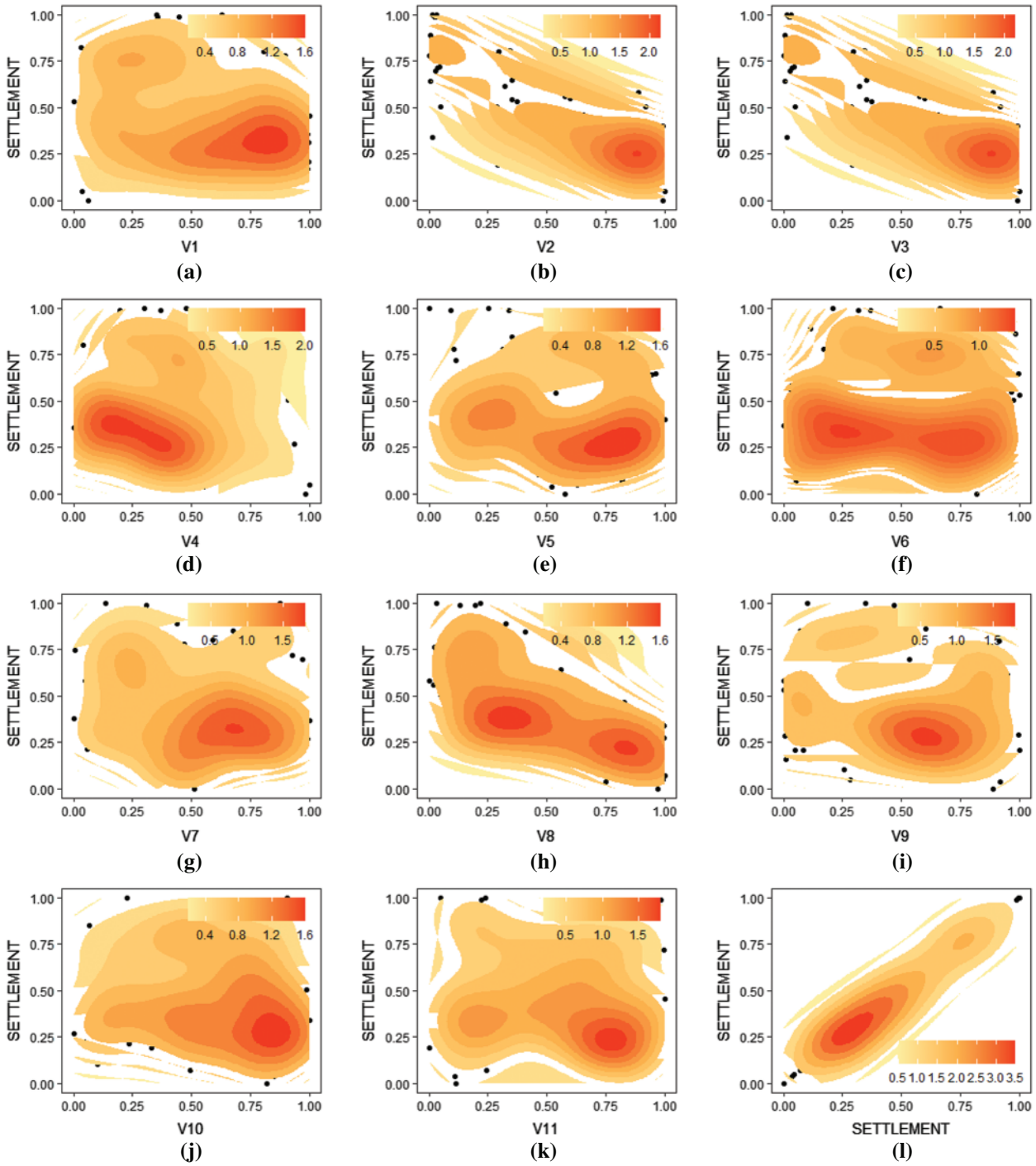

Figure 6: (a–l)—Scatter density plot between input and output variables (V1 to V11 represent input variable from 1 to 11)

6 Results

6.1 Configuration of Developed Models

To determine the structure of the proposed ANN-based hybrid models, it is necessary to select the optimum number of hidden neurons for developing robust models. In the present study, the number of hidden neurons varying from 1 to 15 was examined for conventional ANN. In addition, the log-sigmoid and tan-sigmoid were used as the activation function. Following the trial-and-error approach, the most appropriate number of hidden neurons was obtained as 10 and the tan-sigmoid activation function was more appropriate for ANN-EO and ANN-PSO models. The EO and PSO optimized ANN includes 11 neurons in the input layer, 10 neurons in the hidden layer, and 1 neuron in the output layer (a structure of hybrid ANN model is presented in Fig. 7). The configuration of the proposed hybrid models including the details of population/particle size, the maximum number of iterations, upper and lower bounds, etc., are indicated in Tab. 4 along with the convergence behavior in Fig. 8.

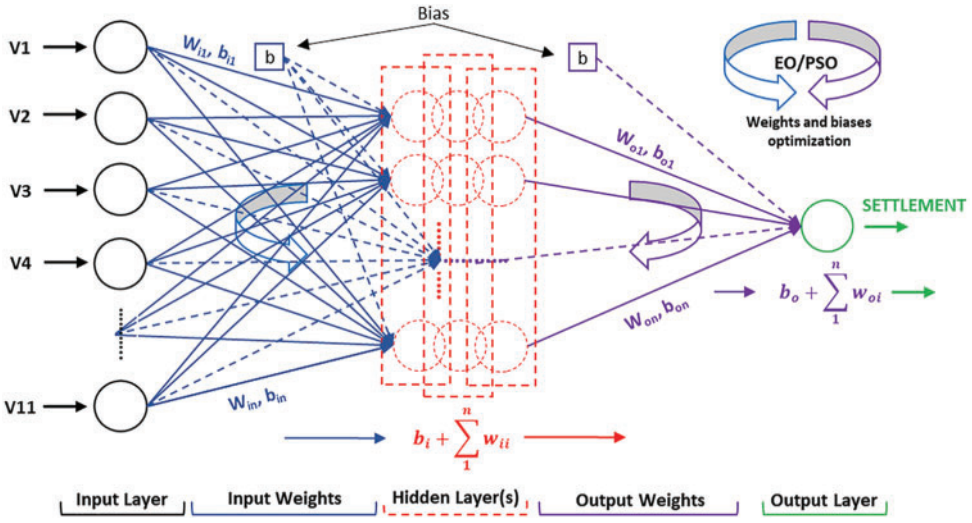

Figure 7: A structure of the developed hybrid ANN model

Table 4: Details of parametric configuration of ANN and ANN-based hybrid models

Parameters	ANN	ANN-EO	ANN-PSO
Input neurons	10	10	10
Hidden neurons	10	10	10
No. of hidden layer	1	1	1
Population/particle size,	–	50	50
Maximum number of iterations	1000	1000	1000
Upper and lower bounds	–	+1, −1	+1, −1
Inertia weights (w_{max}, w_{min})	–	–	0.9, 0.4
Acceleration coefficient (c_1, c_2)	–	1, 2	–
No. of learning parameters	196	196	196
Exploration parameter (a_1)	–	–	2
Exploitation parameter (a_2)	–	–	1

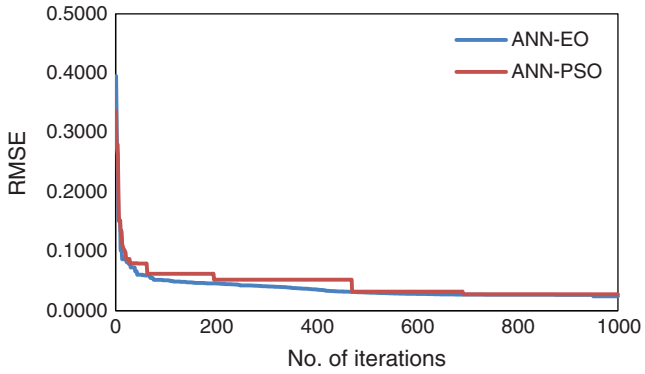

Figure 8: Convergence behavior of ANN-EO and ANN-PSO models

Opposite to the ANN-based models, the parameters of GP and MARS were also designed following the trial-and-error approach. Note that, for constructing an optimum model, the parameters of GP and MARS should be selected suitably. In GP, the parameters are population size, generation number, tournament size, elite fraction, tree depth, number of genes, mutation probability, crossover probability, reproduction probability, etc., while in MARS, number of BFs, GCV per knot, self-interaction, pruning, and aging factor are the most important parameters. It may also be noted that inappropriate values of such parameters increase the complexity of the prediction model, which in turn exhibits poor performance. Tabs. 5 and 6 list the details of GP and MARS parameters obtained through a trial-and-error approach. The following sub-section describes the outcomes of the developed ANN-based models including the GP and MARS in estimating the settlement of PRF, followed by the results of RA and POF.

Table 5: Configuration of GP model

Parameters	Values
Population size	400
Maximum number of generations	150
Tournament size	25
Elite fraction	0.95
Maximum tree depth	4
Maximum no. of genes	6
Mutation probability	0.05
Crossover	0.85
Direct reproduction	0.10
Ephemeral random constants	−10 to +10
Function set	×, +, −, *tanh*, *sin*, *cos*, *exp*

Table 6: Configuration of MARS model

Parameters	Values
GCV penalty per knot (C)	0
Cubic modelling	0 (No)
Self-interactions	1 (No)
Maximum interactions	1
Threshold	1e−04
Prune	1
Artificial ageing factor	0
No. of BFs in the final model	9

6.2 Outcomes of the Developed Models

The prediction outcomes of the developed models in predicting the settlement of PRF are presented in Figs. 9 and 10 for the training dataset, and Figs. 11 and 12 for the testing dataset. Herein, the model performance when it was used to predict the settlement of PRF is reported first. It is noted that model performance with the training dataset was employed to express the goodness of fit of the developed models through the performance parameters, details of which are presented in Tab. 7. Based on the experimental results with the R^2 and RMSE criteria, it can be seen the R^2 values of the developed models lies in the range of 0.9563 to 0.9911 (training stage), while the values of RMSE lies in the range of 0.245 to 0.0542 (training stage). These results clearly demonstrate that the developed models obtained higher prediction performance in estimating the settlement of PRF. In addition, the values of MAE and WI in the training stage were obtained in the range of 0.201 to 0.0381 and 0.9887 to 9978, respectively, which also satisfies higher prediction accuracy. Tab. 7 also represents the outcomes of the developed models for the testing and total dataset. As can be seen, the values of R^2 are higher than 0.90 in the training, testing, and total phases, which indicates that the developed models obtained a good fit to the actual dataset. Among the developed models, the proposed ANN-EO and ANN-PSO models attainted higher prediction accuracy with $R^2 = 0.9911$ and $R^2 = 0.9885$ in the training stage, and, $R^2 = 0.9614$ and $R^2 = 0.9156$ in the testing stage. Overall, the GP and MARS attained the lowest prediction accuracy with $R^2 = 0.9564$ and $R^2 = 0.9518$, respectively.

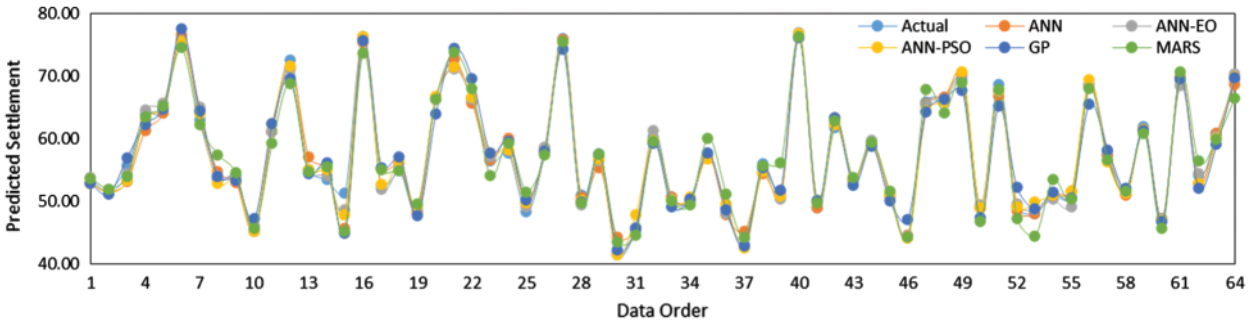

Figure 9: Actual *vs.* predicted settlement values for the training dataset

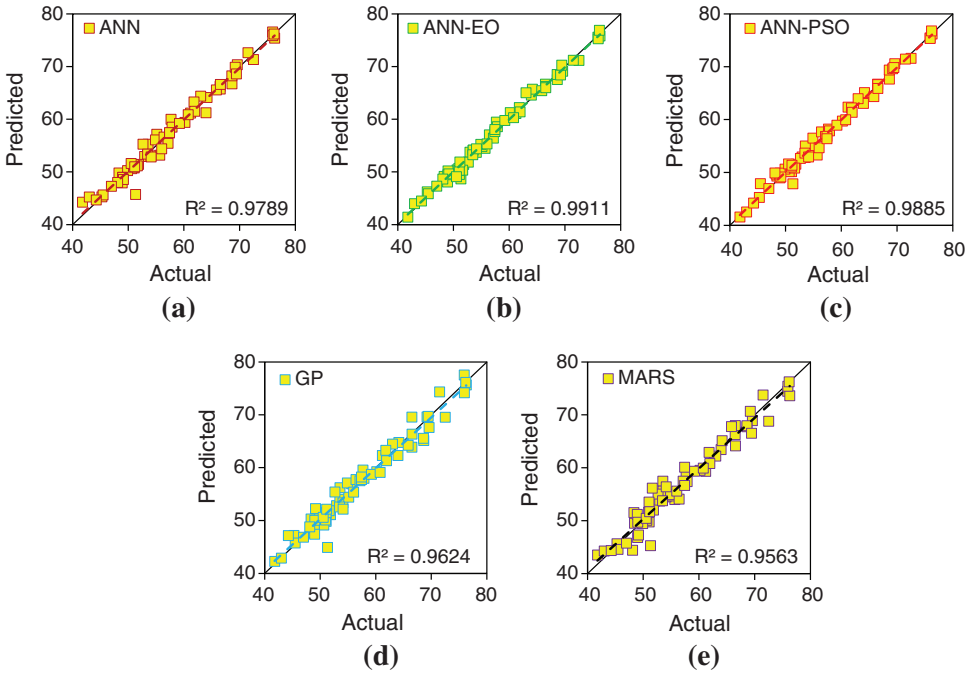

Figure 10: (a–e)—Illustrations of actual and predicted values for the training dataset

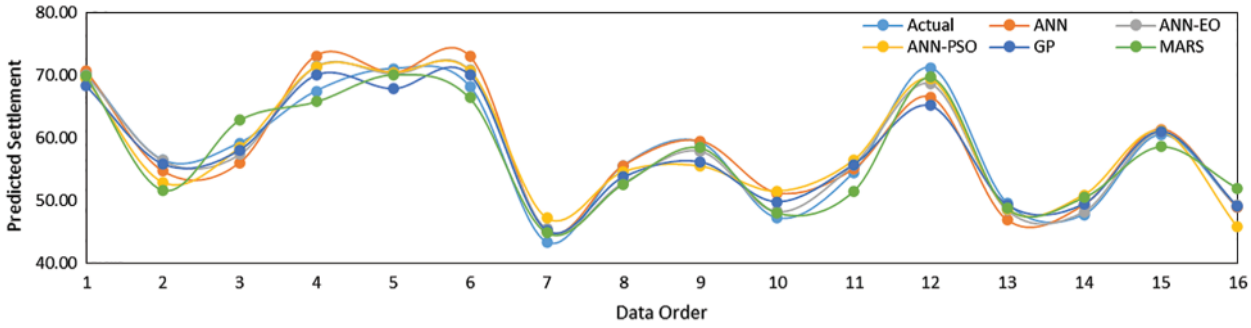

Figure 11: Actual *vs.* predicted settlement values for the testing dataset

The final GP and MARS models are presented in Eqs. (48) and (49), respectively. The GP expression given in Eq. (48) is a combination of 6 genes and a bias term, while the MARS model consists of 9 BFs. The details of BFs are presented in Tab. 8. It may be noted that, although the said models unable to attain the highest prediction accuracy; however, considering the experimental results (R^2, RMSE, and MAE criteria), the developed predictive expressions can readily be used to predict the settlement of PRF. The overall performance of the proposed ANN-EO model was also assessed through rank analysis [79–81], the results of which are presented in Tab. 9. As can be seen, the proposed ANN-EO model attained the highest total rank of 30 and outperformed the other models by far. The MARS and GP are the worst-performing models in this case.

$$S_{pr} = 34.49 \times \{1.796 - 0.2522E_{S0} - 0.1277\,C_{avg} - 0.2522\phi_{avg} - 0.1187\alpha - 0.2616exp(tanh(E_{Sb})) - 0.5311tanh(E_{Sm} + \phi_b) - 0.1081x8(\gamma_{avg} + \phi_b) - 0.2522\gamma_{avg}\} + 41.79 \quad (48)$$

$$S_{pr} = 34.49 \times \{0.40504 - 0.43935 * BF1 + 0.83879 * BF2 - 0.35491 * BF3 + 0.40329 * BF4 + 0.13526 * BF5 - 0.82209 * BF6 - 2.2363 * BF7 + 0.32392 * BF8 + 0.22664 * BF9\} + 41.79 \quad (49)$$

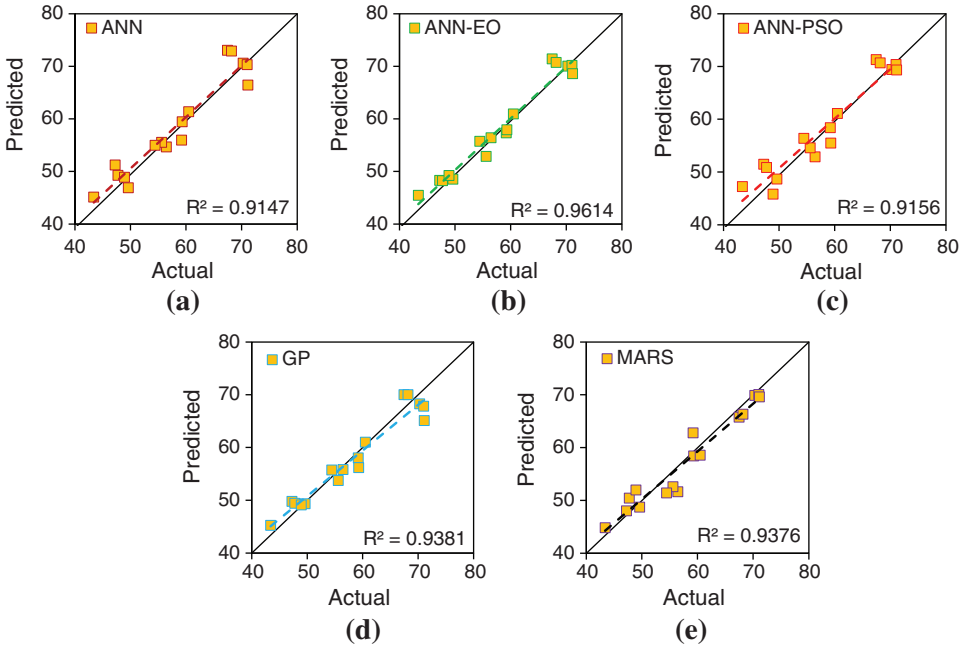

Figure 12: (a–e)—Illustrations of actual and predicted values for the testing dataset

Table 7: Details of performance indices for the training, testing and total dataset

Dataset	Models	R^2	WI	LMI	RMSE	MAE	WMAPE
Training	ANN	0.9789	0.9946	0.8852	0.0377	0.0248	0.0524
	ANN-EO	**0.9911**	**0.9978**	**0.9070**	**0.0245**	**0.0201**	**0.0441**
	ANN-PSO	0.9885	0.9971	0.9054	0.0278	0.0205	0.0450
	GP	0.9624	0.9903	0.8241	0.0503	0.0381	0.0837
	MARS	0.9563	0.9887	0.8084	0.0542	0.0415	0.0899
Testing	ANN	0.9147	0.9771	0.7357	0.0793	0.0592	0.1249
	ANN-EO	**0.9614**	**0.9901**	**0.8144**	**0.0518**	**0.0416**	**0.0877**
	ANN-PSO	0.9156	0.9777	0.7042	0.0766	0.0663	0.1398
	GP	0.9381	0.9805	0.7512	0.0686	0.0558	0.1176
	MARS	0.9376	0.9818	0.7396	0.0677	0.0584	0.1231

(Continued)

Table 7 (continued)

Dataset	Models	R^2	WI	LMI	RMSE	MAE	WMAPE
Total	ANN	0.9649	0.9910	0.8549	0.0489	0.0317	0.0675
	ANN-EO	**0.9850**	**0.9962**	**0.8883**	**0.0319**	**0.0244**	**0.0532**
	ANN-PSO	0.9735	0.9933	0.8644	0.0423	0.0296	0.0647
	GP	0.9564	0.9885	0.8096	0.0544	0.0416	0.0907
	MARS	0.9518	0.9874	0.7948	0.0572	0.0448	0.0968

Table 8: Details of BFs of the developed MARS models

BFs	Expression	BFs	Expression
BF1	max $(0, E_{S0} - 0.29588)$	BF6	max $(0, \phi_{avg} - 0.43788) \times$ max $(0, \gamma_{avg} - 0.28913)$
BF2	max $(0, 0.29588 - E_0)$	BF7	max $(0, \phi_{avg} - 0.43788) \times$ max $(0, 0.28913 - \gamma_{avg})$
BF3	max $(0, \phi_b - 0.46236)$	BF8	max $(0, 0.62845 - E_{Sb})$
BF4	max $(0, 0.46236 - \phi_b)$	BF9	max $(0, 0.81353 - \gamma_{avg})$
BF5	max $(0, 0.60454 - \alpha)$		

Table 9: Results of rank analysis for overall comparison

Models	R^2	WI	LMI	RMSE	MAE	WMAPE	Total rank
ANN	3	3	3	3	3	3	18
ANN-EO	**5**	**5**	**5**	**5**	**5**	**5**	**30**
ANN-PSO	4	4	4	4	4	4	24
GP	2	2	2	2	2	2	16
MARS	1	1	1	1	1	1	8

Tab. 10 reports the values of β of all the developed models, separately for training and testing datasets. Herein, the β of PRF was calculated at different settlement values ranges between 75 and 100 mm. As per IS 1904:1986, permissible settlement of shallow foundations such as raft without pile should be restricted to 75 mm for sandy soil and that of 100 mm for clayey soil. For the present problem, the proposed PRF consists of 26 piles, which are 15 m long and installed in a clayey and sandy medium. Specifically, the first 12 m soils are clayey in nature while below 12 m depth sandy soils are present. Therefore, the values of β were calculated to estimate the POF of the proposed PRF at different values of settlement ranging from 75 to 100 mm. The following steps were followed to determine the β:

(a) Determination of mean settlement value (μ_D) of the observations under consideration. For this study, training and testing observations.
(b) Determination of standard deviation of settlement values (σ_D).
(c) Determination of mean and standard deviation of permissible settlement value, i.e., μ_C and σ_C. For the present scenario, the permissible settlement represents the capacity (C_R) of the proposed PRF.
(d) Determination of β using the expression given in Eq. (26) for the training and testing observations.

Table 10: Values of reliability index at different settlement values

Phase	At settlement (mm)	Actual	ANN	ANN-EO	ANN-PSO	GP	MARS
Training	75	1.95	1.98	1.96	1.97	1.99	2.00
	80	2.51	2.54	2.52	2.52	2.56	2.57
	85	3.06	3.10	3.08	3.08	3.12	3.13
	90	3.62	3.66	3.64	3.64	3.69	3.70
	95	4.17	4.22	4.20	4.20	4.26	4.27
	100	4.73	4.78	4.75	4.76	4.82	4.84
Testing	75	1.81	1.72	1.80	1.82	2.06	2.00
	80	2.35	2.25	2.33	2.37	2.66	2.57
	85	2.88	2.77	2.87	2.91	3.26	3.15
	90	3.42	3.30	3.41	3.46	3.87	3.72
	95	3.96	3.82	3.94	4.01	4.47	4.30
	100	4.49	4.35	4.48	4.56	5.07	4.87

Table 11: Values of POF at different settlement values

Phase	At settlement (mm)	Actual	ANN	ANN-EO	ANN-PSO	GP	MARS
Training	75	2.53	2.41	2.48	2.46	2.32	2.28
	80	0.60	0.56	0.58	0.58	0.53	0.51
	85	0.11	0.10	0.10	0.10	0.09	0.09
	90	**0.01**	**0.01**	**0.01**	**0.01**	**0.01**	**0.01**
	95	**0.00**	**0.00**	**0.00**	**0.00**	**0.00**	**0.00**
	100	**0.00**	**0.00**	**0.00**	**0.00**	**0.00**	**0.00**
Testing	75	3.52	4.23	3.62	3.44	1.96	2.28
	80	0.95	1.23	0.98	0.90	0.39	0.50
	85	0.20	0.28	0.21	0.18	0.05	0.08
	90	**0.03**	**0.05**	**0.03**	**0.03**	**0.01**	**0.01**
	95	**0.00**	**0.01**	**0.00**	**0.00**	**0.00**	**0.00**
	100	**0.00**	**0.00**	**0.00**	**0.00**	**0.00**	**0.00**

Subsequently, the POF of the proposed PRF was determined using the expression given in Eq. (27), separately for training and testing datasets, the details of which are reported in Tab. 11. Note that, the values of POF reported herein are in percentage term. From the results presented in Tabs. 10 and 11, it is clearly observed that the proposed ANN-EO and ANN-PSO able to estimate the risk associated with the proposed PRF in terms of β and POF. Figs. 13–15 represent the values of β at different settlement values for the developed models; while Figs. 16–18 represent the details of POF of the proposed PRF. As can be seen, the values of β are closer to the actual value for the ANN-EO (1.95 *vs*. 1.96 at 75 mm settlement and 4.73 *vs*. 4.75 at 100 mm settlement) and ANN-PSO (1.95 *vs*. 1.97 at 75 mm settlement and 4.73 *vs*. 4.76 at 100 mm settlement) in the training stage; while in the testing stage. 1.81 *vs*. 1.80 at 75 mm settlement and 4.49 *vs*. 4.48 at

100 mm settlement (for ANN-EO) and 1.81 *vs*. 1.82 at 75 mm settlement and 4.49 *vs*. 4.56 at 100 mm settlement (for ANN-PSO). Also, the values of POF calculated at different settlement values are in line with the actual values of POF.

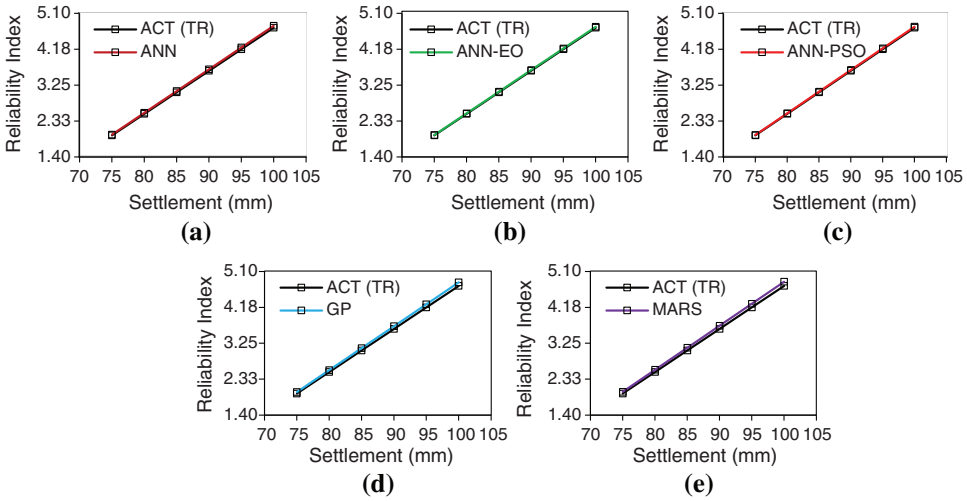

Figure 13: (a–e)—Settlement *vs*. Reliability Index plot for the training dataset (model wise)

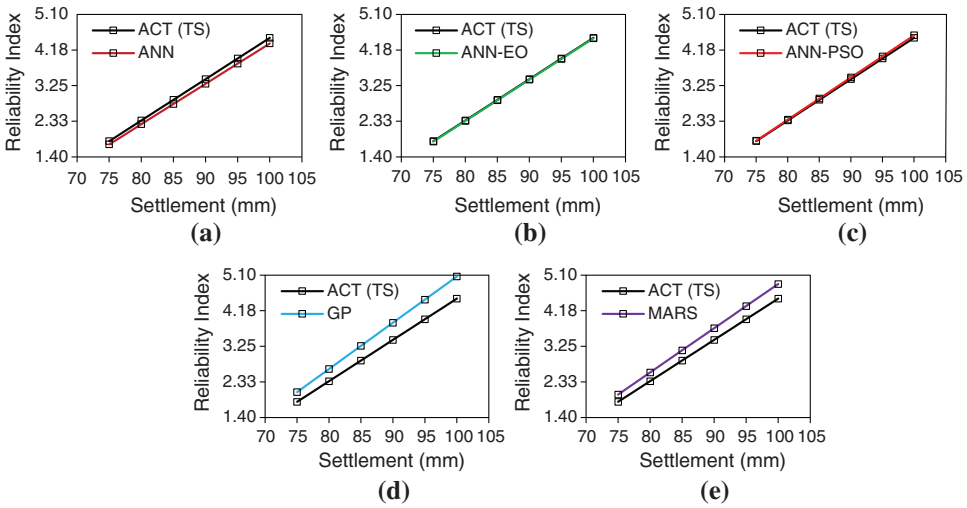

Figure 14: (a–e)—Settlement *vs*. Reliability Index plot for the testing dataset (model wise)

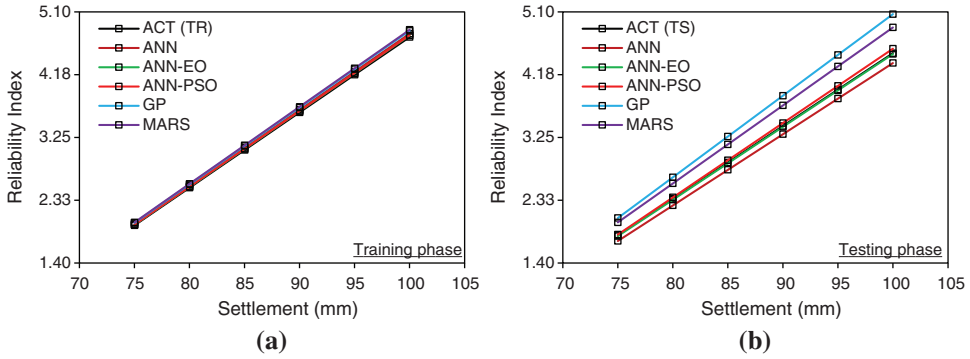

Figure 15: (a–b)—Settlement *vs*. Reliability Index plot (all models together)

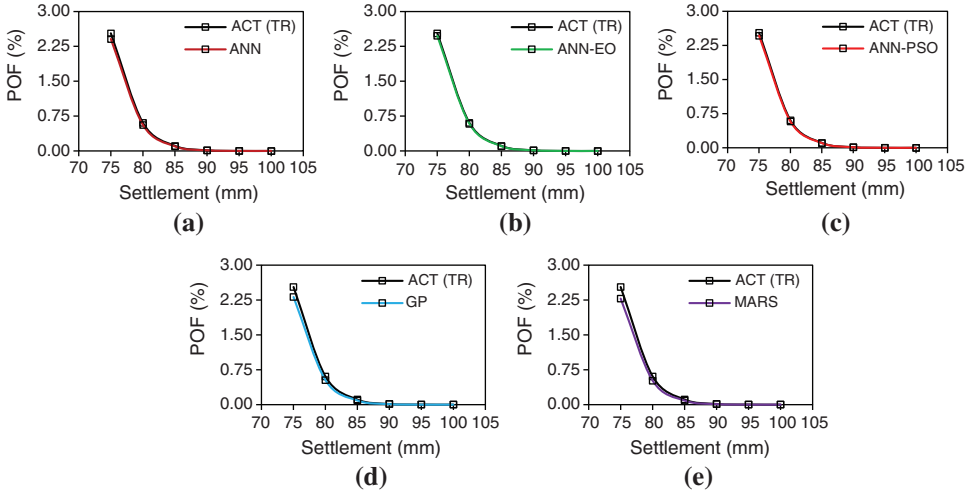

Figure 16: (a–e)—Settlement *vs*. Probability of failure plot for the testing dataset (model wise)

7 Discussion

As mentioned earlier, the proposed PRF consists of 26 piles and all piles are 15 m long. The top 12 m is embedded in the clayey layer while the bottom 3 m is resting in sandy soil. The present problem, the settlement of raft foundation (without piles) was estimated as 113.68 mm, which exceeds the permissible value of 100 mm as per IS 1904–1986. Note that, if the estimated settlement of raft foundation is greater than the permissible limit, it would be necessary to introduce piles as a measure of settlement reducer. Therefore, to restrict the settlement within the permissible value, a combination of raft and piles, i.e., PRF was selected as the foundation type. For the same conditions, the revised settlement was calculted as 66.08 mm only. However, to investigate the failure probability of the proposed PRF in a more comprehensive manner, values of β at different permissible settlements ranging from 75 to 100 mm were determined. Based on the calculated results, it was seen that the values of POF generated through ANN-EO and ANN-PSO truly reflect the actual POF in both stages. No deviation was observed in the range of 90 to 100 mm permissible settlement value. The actual values of POF were calculated between 0% and 0.01% in the training stage and that of 0% and 0.03% in the testing phase. Graphical

plots presented in Figs. 13–18 depict the comparison of the actual and modelled values of β and POF of the developed models, including the proposed ANN-EO and ANN-PSO. It is clearly shown that the proposed ANN-EO reliably estimate the β and its corresponding POF of the PRF in both stages. The same conclusion can be drawn for the other developed models where the estimated POF are in line with the actual value in the training stage; however, the ANN, GP, and MARS show slight deviation in the testing phase. These results clearly indicate overfitting-related issues of the traditional soft computing techniques in predicting the desired output for the new dataset. In the present study, the proposed ANN-EO and ANN-PSO show better results, which in turn indicates that the incorporation of meta-heuristic algorithms improves the performance of traditional ANN by far. Overall, the ANN-EO predicts the risk associated with the proposed PRF in both stages, followed by ANN-PSO, ANN, GP, and MARS.

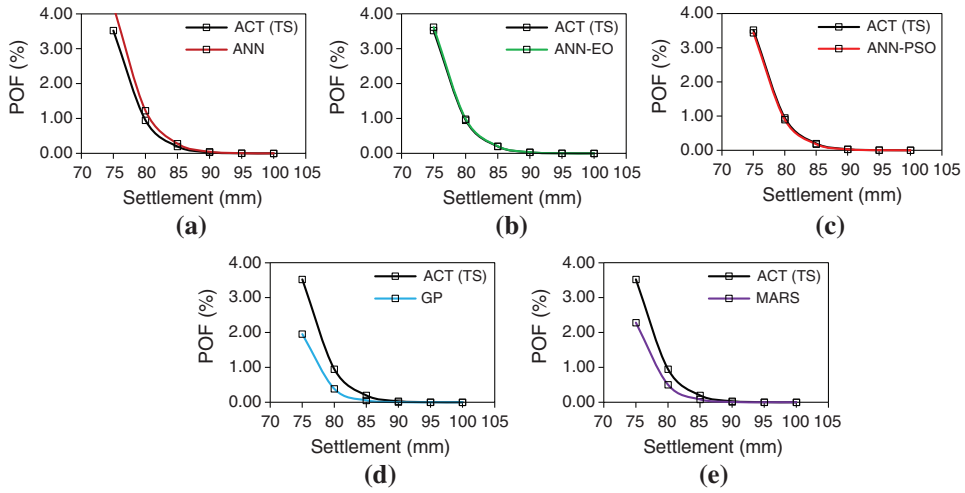

Figure 17: (a–e)—Settlement *vs.* Probability of failure plot for the testing dataset (model wise)

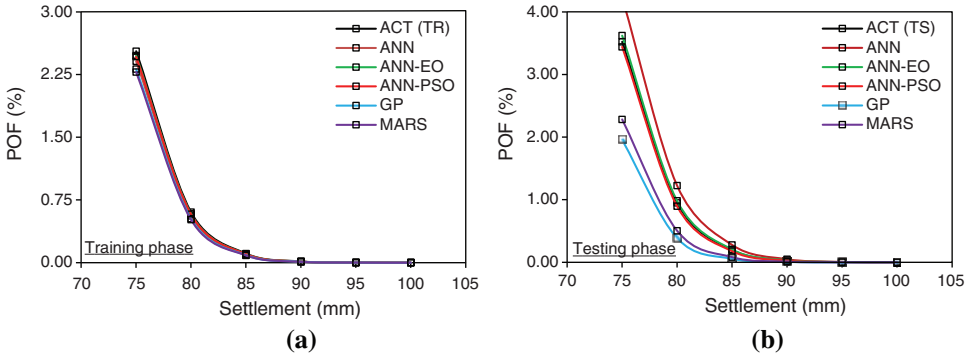

Figure 18: (a–b)—Settlement *vs.* Probability of failure plot (all models together)

8 Conclusion

This study presents a high-performance soft computing technique to perform the RA of PRF. The proposed model is a combination of the classical ANN and EO, i.e., ANN-EO. Initially, the

ANN-EO was employed to construct a prediction model for estimating the settlement of PRF from a set of 11 influencing factors. Later, the ANN-EO along with other developed models (ANN, MARS, GP, and ANN-PSO) were used to investigate the risk associated with the PRF in terms of POF. The failure probability of PRF with cantilever retailing wall arrangement was investigated for a set of settlement values ranging from 75 to 100 mm. This was done to investigate the inter-relationship between the settlement and POF for the proposed PRF. The theoretical analysis suggested that the proposed PRF attained almost negligible failure probability (in the range of 0.01% to 0.03%) at 90 mm or more permissible settlement value. Therefore, the proposed PRF could be considered safe against settlement failure at a designed permissible settlement value of 90 mm.

All the proposed models demonstrate higher prediction results to the actual POF in the training phase, while the proposed hybrid ANN-EO model attained the most desired prediction value with $R^2 = 0.9911$, RMSE = 0.0245, and MAE = 0.0201 in the training stage, and $R^2 = 0.9614$, RMSE = 0.0518, and MAE = 0.0416 in the testing phase. These outcomes are significantly better than those obtained from ANN-PSO, including the traditional ANN, GP, and MARS used to estimate the failure probability of the proposed PRF. The computational cost of the proposed ANN-EO and ANN-PSO was recorded as 421.860941 s and 429.964295 s, respectively, using MATLAB environment with MATLAB 2015a, i7-4790 CPU @ 3.60 GHz, 8 GB RAM. The main advantages of the proposed ANN-EO model include higher prediction accuracy, ease of implementation using the existing dataset, and high generalization capability. The future direction of this study may include a) integration of ANN and other meta-heuristic OAs and a detailed comparison of ANN-EO with other hybrid ANN models, b) use of deep learning models and construction of hybrid models of deep learning models and meta-heuristic OAs, c) selection of input parameters using feature selection techniques, d) implementation of dimension reduction procedure and inter-quartile technique to handle noise in the dataset, and e) reduction of computational costs using an enhanced version of OAs. In addition, implementation of other reliability-based analyses to compare the results of FORM and the developed models in detail. Nevertheless, the concept proposed in this study can be used to perform RA of other civil engineering structures; however, the existing database should be prepared before the estimation of the reliability index and its corresponding POF. Based on these facts, the proposed ANN-EO can be used as a promising alternative to estimate the POF of PRF, including many other civil engineering structures. As per the authors' knowledge, the implementation of hybrid ANN models, specifically ANN-EO for performing the reliability analysis of PRF would significantly contribute to the knowledge pool of reliability studies related to PRF due to the fact that the literature on reliability analysis of PRS is relatively scarce.

Author's Contributions: **A. Bardhan:** Main author, conceptualization, overall analysis, development of AI models, detailing, and manuscript finalization; **P. Manna:** Theoretical analysis; **V. Kumar:** Referencing; **A. Burman:** Overall review; **B. Žlender:** Overall review; **P. Samui:** Overall review.

Funding Statement: The authors received no specific funding for this study.

Conflicts of Interest: The authors declare that they have no conflicts of interest to report regarding the present study.

References

1. Al-Kinani, A. S. H. R. A. F., Reddy, D. E. S. (2014). Design of the piled raft foundations for load settlement behavior using a multiphase model. *International Journal of Scientific Enginh. keering and Technology, 3,* 4766–4776. http://ijsetr.com/uploads/514326IJSETR2097-842.pdf.
2. Ghorbani, A., Firouzi Niavol, M. (2017). Evaluation of induced settlements of piled rafts in the coupled static-dynamic loads using neural networks and evolutionary polynomial regression. *Applied Computational Intelligence and Soft Computing, 2017(2),* 1–23. DOI 10.1155/2017/7487438.
3. Niandou, H., Breysse, D. (2007). Reliability analysis of a piled raft accounting for soil horizontal variability. *Computers and Geotechnics, 34(2),* 71–80. DOI 10.1016/j.compgeo.2006.09.006.
4. Griffiths, D. V., Clancy, P., Randolph, M. F. (1991). Piled raft foundation analysis by finite elements. *International Conference on Computer Methods and Advances in Geomechanics*, vol. 7, pp. 1153–1157. Cairns, Australia.
5. Horikoshi, K., Randolph, M. F. (1998). A contribution to optimum design of piled rafts. *Geotechnique, 48(3),* 301–317. DOI 10.1680/geot.1998.48.3.301.
6. Poulos, H. G. (1994). An approximate numerical analysis of pile-raft interaction. *International Journal for Numerical and Analytical Methods in Geomechanics, 18(2),* 73–92. DOI 10.1002/(ISSN)1096-9853.
7. Brzakała, W., Puła, W. (1996). A probabilistic analysis of foundation settlements. *Computers and Geotechnics, 18(4),* 291–309. DOI 10.1016/0266-352X(95)00033-7.
8. Russo, G. (1998). Numerical analysis of piled rafts. *International Journal for Numerical and Analytical Methods in Geomechanics, 22(6),* 477–493. DOI 10.1002/(ISSN)1096-9853.
9. Kim, K. N., Lee, S. H., Kim, K. S., Chung, C. K., Kim, M. M. et al. (2001). Optimal pile arrangement for minimizing differential settlements in piled raft foundations. *Computers and Geotechnics, 28(4),* 235–253. DOI 10.1016/S0266-352X(01)00002-7.
10. Davis, E. H., Poulos, H. G. (1972). The analysis of piled raft systems. *Australian Geomech Journal G2,* 21–27.
11. Clancy, P., Randolph, M. F. (1996). Simple design tools for piled raft foundations. *Geotechnique, 46(2),* 313–328. DOI 10.1680/geot.1996.46.2.313.
12. Kumar, M., Samui, P. (2019). Reliability analysis of pile foundation using ELM and MARS. *Geotechnical and Geological Engineering, 37(4),* 3447–3457. DOI 10.1007/s10706-018-00777-x.
13. Duncan, J. M. (2000). Factors of safety and reliability in geotechnical engineering. *Journal of Geotechnical and Geoenvironmental Engineering, 126(4),* 307–316. DOI 10.1061/(ASCE)1090-0241(2000)126:4(307).
14. Kumar, M., Samui, P. (2020). Reliability analysis of settlement of pile group in clay using LSSVM, GMDH. *GPR Geotechnical and Geological Engineering, 38(6),* 6717–6730. DOI 10.1007/s10706-020-01464-6.
15. Kumar, M., Samui, P., Kumar, D., Zhang, W. (2021). Reliability analysis of settlement of pile group. *Innovative Infrastructure Solutions, 6(1),* 1–17.
16. Kumar, M., Bardhan, A., Samui, P., Hu, J. W., Kaloop, R. et al. (2021). Reliability analysis of pile foundation using soft computing techniques: A comparative study. *Processes, 9(3),* 486. DOI 10.3390/pr9030486.
17. Kumar, R., Samui, P., Kumari, S., Roy, S. S. (2021). Determination of reliability index of cantilever retaining wall by RVM, MPMR and MARS. *International Journal of Advanced Intelligence Paradigms, 18(3),* 316–336. DOI 10.1504/IJAIP.2021.113325.
18. Kumar, R., Samui, P., Kumari, S., Dalkilic, Y. H. (2021). Reliability analysis of circular footing by using GP and MPMR. *International Journal of Applied Metaheuristic Computing, 12(1),* 1–19. DOI 10.4018/IJAMC.
19. Ray, R., Kumar, D., Samui, P., Roy, L. B., Goh, A. T. C. et al. (2021). Application of soft computing techniques for shallow foundation reliability in geotechnical engineering. *Geoscience Frontiers, 12(1),* 375–383. DOI 10.1016/j.gsf.2020.05.003.
20. Tawfik, M. E., Bishay, P. L., Sadek, E. A. (2018). Neural network-based second order reliability method (NNBSORM) for laminated composite plates in free vibration. *Computer Modeling in Engineering & Sciences, 115(1),* 105–129. DOI 10.3970/cmes.2018.115.105.
21. Kerh, T., Lai, J. S., Gunaratnam, D., Saunders, R. (2008). Evaluation of seismic design values in the Taiwan building code by using artificial neural network. *Computer Modeling in Engineering & Sciences, 26(1),* 1. https://www.techscience.com/CMES/v26n1/25101.

22. Karaci, A., Yaprak, H., Ozkaraca, O., Demir, I., Simsek, O. (2019). Estimating the properties of ground-waste-brick mortars using DNN and ANN. *Computer Modeling in Engineering & Sciences, 118(1),* 207–228. DOI 10.31614/cmes.2019.04216.
23. Roy, B., Singh, M. P. (2020). An empirical-based rainfall-runoff modelling using optimization technique. *International Journal of River Basin Management, 18(1),* 49–67. DOI 10.1080/15715124.2019.1680557.
24. Koopialipoor, M., Fallah, A., Armaghani, D. J., Azizi, A., Mohamad, E. T. (2019). Three hybrid intelligent models in estimating flyrock distance resulting from blasting. *Engineering with Computers, 35(1),* 243–256. DOI 10.1007/s00366-018-0596-4.
25. Livingstone, D. J., Manallack, D. T., Tetko, I. V. (1996). Data modeling with neural networks—An answer to the maiden's prayer. *Journal of Computer-Aided Molecular Design, 11(2),* 135–142. DOI 10.1023/A:1008074223811.
26. Mishra, M., Srivastava, M. (2014). A view of artificial neural network. *2014 International Conference on Advances in Engineering & Technology Research*, pp. 1–3. Unnao, India, IEEE. DOI 10.1109/ICAETR.2014.7012785.
27. Liou, S. W., Wang, C. M., Huang, Y. F. (2009). Integrative discovery of multifaceted sequence patterns by frame-relayed search and hybrid PSO-ANN. *Journal of Universal Computer Science, 15(4),* 742–764. DOI 10.3217/jucs-015-04-0742.
28. Moayedi, H., Moatamediyan, A., Nguyen, H., Bui, X. N., Bui, D. T. et al. (2020). Prediction of ultimate bearing capacity through various novel evolutionary and neural network models. *Engineering with Computers, 36(2),* 671–687. DOI 10.1007/s00366-019-00723-2.
29. Le, L. T., Nguyen, H., Dou, J., Zhou, J. (2019). A comparative study of PSO-ANN, GA-ANN, ICA-ANN, and ABC-ANN in estimating the heating load of buildings' energy efficiency for smart city planning. *Applied Sciences, 9(13),* 2630. DOI 10.3390/app9132630.
30. Bui, D. T., Nhu, V. H., Hoang, N. D. (2018). Prediction of soil compression coefficient for urban housing project using novel integration machine learning approach of swarm intelligence and multi-layer perceptron neural network. *Advanced Engineering Informatics, 38,* 593–604. DOI 10.1016/j.aei.2018.09.005.
31. Fattahi, H., Bayatzadehfard, Z. (2018). Forecasting surface settlement caused by shield tunneling using ANN-BBO model and ANFIS based on clustering methods. *Journal of Engineering Geology, 12,* 55. DOI 10.18869/acadpub.jeg.12.5.55.
32. Nguyen, M. D., Pham, B. T., Ho, L. S., Ly, H. B., Le, T. T. et al. (2020). Soft-computing techniques for prediction of soils consolidation coefficient. *Catena, 195,* 104802. DOI 10.1016/j.catena.2020.104802.
33. Akbal, B. (2018). GSA-ANN and DEA-ANN methods to prevent underground cable line faults. *International Journal of Computer and Electrical Engineering, 10(2),* 85–93. DOI 10.17706/IJCEE.2018.10.2.85-93.
34. Rao, A. N., Vijayapriya, P. (2019). A robust neural network model for monitoring online voltage stability. *International Journal of Computers and Applications, 41,* 1–10. DOI 10.1080/1206212X.2019.1666224.
35. Yang, Z. C., Sun, W. C. (2013). A set-based method for structural eigenvalue analysis using Kriging model and PSO algorithm. *Computer Modeling in Engineering & Sciences, 92(2),* 193–212. DOI 10.3970/cmes.2013.092.193.
36. Hou, G., Xu, Z., Liu, X., Jin, C. (2019). Improved particle swarm optimization for selection of shield tunneling parameter values. *Computer Modeling in Engineering & Sciences, 118(2),* 317–337. DOI 10.31614/cmes.2019.04693.
37. Sunil, N., Ganesan, R., Sankaragomathi, B. (2019). Analysis of OSA syndrome from PPG signal using CART-PSO classifier with time domain and frequency domain features. *Computer Modeling in Engineering & Sciences, 118(2),* 351–375. DOI 10.31614/cmes.2018.04484.
38. Hasanipanah, M., Shahnazar, A., Amnieh, H. B., Armaghani, D. J. (2017). Prediction of air-overpressure caused by mine blasting using a new hybrid PSO-SVR model. *Engineering with Computers, 33(1),* 23–31. DOI 10.1007/s00366-016-0453-2.
39. Sujith, M., Padma, S. (2020). Implementation of PSOANN optimized PI control algorithm for shunt active filter. *Computer Modeling in Engineering & Sciences, 122(3),* 863–888. DOI 10.32604/cmes.2020.08908.

40. Li, G., Kumar, D., Samui, P., Nikafshan Rad, H., Roy, B. et al. (2020). Developing a new computational intelligence approach for approximating the blast-induced ground vibration. *Applied Sciences, 10(2),* 434. DOI 10.3390/app10020434.
41. Kaloop, M. R., Kumar, D., Zarzoura, F., Roy, B., Hu, J. W. (2020). A wavelet-particle swarm optimization-extreme learning machine hybrid modeling for significant wave height prediction. *Ocean Engineering, 213(11),* 107777. DOI 10.1016/j.oceaneng.2020.107777.
42. Ly, H. B., Pham, B. T., Le, L. M., Le, T. T., Le, V. M. et al. (2021). Estimation of axial load-carrying capacity of concrete-filled steel tubes using surrogate models. *Neural Computing and Applications, 33(8),* 3437–3458. DOI 10.1007/s00521-020-05214-w.
43. Hajihassani, M., Armaghani, D. J., Sohaei, H., Mohamad, E. T., Marto, A. (2014). Prediction of airblast-overpressure induced by blasting using a hybrid artificial neural network and particle swarm optimization. *Applied Acoustics, 80,* 57–67. DOI 10.1016/j.apacoust.2014.01.005.
44. Armaghani, D. J., Hajihassani, M., Mohamad, E. T., Marto, A., Noorani, S. A. (2014). Blasting-induced flyrock and ground vibration prediction through an expert artificial neural network based on particle swarm optimization. *Arabian Journal of Geosciences, 7(12),* 5383–5396. DOI 10.1007/s12517-013-1174-0.
45. Golafshani, E. M., Behnood, A., Arashpour, M. (2020). Predicting the compressive strength of normal and high-performance concretes using ANN and ANFIS hybridized with grey wolf optimizer. *Construction and Building Materials, 232(4),* 117266. DOI 10.1016/j.conbuildmat.2019.117266.
46. Hasanipanah, M., Armaghani, D. J., Amnieh, H. B., Abd Majid, M. Z., Tahir, M. M. (2017). Application of PSO to develop a powerful equation for prediction of flyrock due to blasting. *Neural Computing and Applications, 28(1),* 1043–1050. DOI 10.1007/s00521-016-2434-1.
47. Zhou, X., Armaghani, D. J., Ye, J., Khari, M., Motahari, M. R. (2021). Hybridization of parametric and non-parametric techniques to predict air over-pressure induced by quarry blasting. *Natural Resources Research, 30(1),* 209–224. DOI 10.1007/s11053-020-09714-3.
48. Rad, H. N., Bakhshayeshi, I., Jusoh, W. A. W., Tahir, M. M., Foong, L. K. (2020). Prediction of flyrock in mine blasting: A new computational intelligence approach. *Natural Resources Research, 29(2),* 609–623. DOI 10.1007/s11053-019-09464-x.
49. Faramarzi, A., Heidarinejad, M., Stephens, B., Mirjalili, S. (2020). Equilibrium optimizer: A novel optimization algorithm. *Knowledge-Based Systems, 191,* 105190. DOI 10.1016/j.knosys.2019.105190.
50. Elsheikh, A. H., Shehabeldeen, T. A., Zhou, J., Showaib, E., Abd Elaziz, M. (2021). Prediction of laser cutting parameters for polymethylmethacrylate sheets using random vector functional link network integrated with equilibrium optimizer. *Journal of Intelligent Manufacturing, 32(5),* 1377–1388. DOI 10.1007/s10845-020-01617-7.
51. Foong, L. K., Moayedi, H. (2021). Slope stability evaluation using neural network optimized by equilibrium optimization and vortex search algorithm. *Engineering with Computers, 37(3),* 1–15. DOI 10.1007/s00366-021-01282-1.
52. Agnihotri, S., Atre, A., Verma, H. K. (2020). Equilibrium optimizer for solving economic dispatch problem. *IEEE 9th Power India International Conference*, pp. 1–5. Sonepat, India, IEEE. DOI 10.1109/PIICON49524.2020.9113048.
53. Randolph, M. F., Wroth, C. P. (1978). Analysis of deformation of vertically loaded piles. *Journal of the Geotechnical Engineering Division, 104(12),* 1465–1488. DOI 10.1061/AJGEB6.0000729.
54. Burland, J. B. (1970). Discussion of session A. *Proceedings of the Conference on in situ Investigation in Soils and Rocks, British Geotechnical Society*, pp. 61–62. London, England.
55. Fleming, W. G. K., Weltman, A. J., Randolph, M. F., Elson, W. K. (1992). *Piling engineering*. 2nd ed. Blackie, Glasgow & London.
56. Poulos, H. G., Davis, E. H. (1980). *Pile foundation analysis and design*. New York: Wiley.
57. Mayne, P. W., Poulos, H. G. (1999). Approximate displacement influence factors for elastic shallow foundations. *Journal of Geotechnical and Geoenvironmental Engineering, 125(6),* 453–460. DOI 10.1061/(ASCE)1090-0241(1999)125:6(453).

58. Haldar, A., Mahadevan, S. (1995). First-order and second-order reliability methods. *Probabilistic structural mechanics handbook,* pp. 27–52. Boston, MA: Springer.
59. Du, X. (2008). Unified uncertainty analysis by the first order reliability method. *Journal of Mechanical Design, 130(9),* 171. DOI 10.1115/1.2943295.
60. Maier, H. R., Lence, B. J., Tolson, B. A., Foschi, R. O. (2001). First-order reliability method for estimating reliability, vulnerability, and resilience. *Water Resources Research, 37(3),* 779–790. DOI 10.1029/2000WR900329.
61. Low, B. K., Tang, W. H. (2007). Efficient spreadsheet algorithm for first-order reliability method. *Journal of Engineering Mechanics, 133(12),* 1378–1387. DOI 10.1061/(ASCE)0733-9399(2007)133:12(1378).
62. Baecher, G. B., Christian, J. T. (2005). *Reliability and statistics in geotechnical engineering*. Hoboken, New Jersey: John Wiley & Sons.
63. Kurugodu, H. V., Bordoloi, S., Hong, Y., Garg, A., Garg, A. et al. (2018). Genetic programming for soil-fiber composite assessment. *Advances in Engineering Software, 122(8),* 50–61. DOI 10.1016/j.advengsoft.2018.04.004.
64. Gandomi, A. H., Alavi, A. H. (2012). A new multi-gene genetic programming approach to nonlinear system modeling. Part I: Materials and structural engineering problems. *Neural Computing and Applications, 21(1),* 171–187. DOI 10.1007/s00521-011-0734-z.
65. Gandomi, A. H., Alavi, A. H. (2012). A new multi-gene genetic programming approach to non-linear system modeling. Part II: Geotechnical and earthquake engineering problems. *Neural Computing and Applications, 21(1),* 189–201. DOI 10.1007/s00521-011-0735-y.
66. Koza, J. R. (1992), *Genetic programming: On the programming of computers by means of natural selection*, vol. 1. Cambridge, Massachusetts: MIT Press.
67. Emamian, S. A., Eskandari-Naddaf, H. (2020). Genetic programming based formulation for compressive and flexural strength of cement mortar containing nano and micro silica after freeze and thaw cycles. *Construction and Building Materials, 241,* 118027. DOI 10.1016/j.conbuildmat.2020.118027.
68. Ghani, S., Kumari, S., Choudhary, A. K., Jha, J. N. (2021). Experimental and computational response of strip footing resting on prestressed geotextile-reinforced industrial waste. *Innovative Infrastructure Solutions, 6(2),* 1–15. DOI 10.1007/s41062-021-00468-2.
69. Sadat-Noori, M., Glamore, W., Khojasteh, D. (2020). Groundwater level prediction using genetic programming: The importance of precipitation data and weather station location on model accuracy. *Environmental Earth Sciences, 79(1),* 1–10. DOI 10.1007/s12665-019-8776-0.
70. Zhang, Q., Barri, K., Jiao, P., Salehi, H., Alavi, A. H. (2021). Genetic programming in civil engineering: Advent, applications and future trends. *Artificial Intelligence Review, 54(3),* 1863–1885. DOI 10.1007/s10462-020-09894-7.
71. Hien, N. T., Tran, C. T., Nguyen, X. H., Kim, S., Phai, V. D. et al. (2020). Genetic programming for storm surge forecasting. *Ocean Engineering, 215(3),* 107812. DOI 10.1016/j.oceaneng.2020.107812.
72. Biswas, R., Rai, B., Samui, P., Roy, S. S. (2020). Estimating concrete compressive strength using MARS, LSSVM and GP. *Engineering Journal, 24(2),* 41–52. DOI 10.4186/ej.2020.24.2.41.
73. Cheng, Z. L., Zhou, W. H., Garg, A. (2020). Genetic programming model for estimating soil suction in shallow soil layers in the vicinity of a tree. *Engineering Geology, 268(1),* 105506. DOI 10.1016/j.enggeo.2020.105506.
74. Aslam, F., Farooq, F., Amin, M. N., Khan, K., Waheed, A. et al. (2020). Applications of gene expression programming for estimating compressive strength of high-strength concrete. *Advances in Civil Engineering, 2020(3),* 1–23. DOI 10.1155/2020/8850535.
75. Akin, O. O., Ocholi, A., Abejide, O. S., Obari, J. A. (2020). Prediction of the compressive strength of concrete admixed with metakaolin using gene expression programming. *Advances in Civil Engineering, 2020(2),* 1–7. DOI 10.1155/2020/8883412.
76. Friedman, J. H. (1991). Multivariate adaptive regression splines. *The Annals of Statistics, 19(1),* 1–67. DOI 10.1214/aos/1176347963.

77. Cai, M., Koopialipoor, M., Armaghani, D. J., Thai Pham, B. (2020). Evaluating slope deformation of earth dams due to earthquake shaking using MARS and GMDH techniques. *Applied Sciences, 10(4),* 1486. DOI 10.3390/app10041486.
78. Kennedy, J., Eberhart, R. (1995). Particle swarm optimization. *Proceedings of ICNN'95-International Conference on Neural Networks*, vol. 4, pp. 1942–1948. Perth, WA, Australia, IEEE.
79. Asteris, P. G., Skentou, A. D., Bardhan, A., Samui, P., Pilakoutas, K. (2021). Predicting concrete compressive strength using hybrid ensembling of surrogate machine learning models. *Cement and Concrete Research, 145(3),* 106449. DOI 10.1016/j.cemconres.2021.106449.
80. Kardani, N., Bardhan, A., Samui, P., Nazem, M., Zhou, A. et al. (2021). A novel technique based on the improved firefly algorithm coupled with extreme learning machine (ELM-IFF) for predicting the thermal conductivity of soil. *Engineering with Computers*. DOI 10.1007/s00366-021-01329-3.
81. Kardani, N., Bardhan, A., Kim, D., Samui, P., Zhou, A. (2021). Modelling the energy performance of residential buildings using advanced computational frameworks based on RVM, GMDH, ANFIS-BBO and ANFIS-IPSO. *Journal of Building Engineering, 35(10),* 102105. DOI 10.1016/j.jobe.2020.102105.
82. Kardani, M. N., Baghban, A., Hamzehie, M. E., Baghban, M. (2019). Phase behavior modeling of asphaltene precipitation utilizing RBF-ANN approach. *Petroleum Science and Technology, 37(16),* 1861–1867. DOI 10.1080/10916466.2017.1289222.
83. Ghani, S., Kumari, S., Bardhan, A. (2021). A novel liquefaction study for fine-grained soil using PCA-based hybrid soft computing models. *Sādhanā, 46(3),* 1–17. DOI 10.1007/s12046-021-01640-1.
84. Bardhan, A., Gokceoglu, C., Burman, A., Samui, P., Asteris, P. G. (2021). Efficient computational techniques for predicting the California bearing ratio of soil in soaked conditions. *Engineering Geology, 291,* 106239. DOI 10.1016/j.enggeo.2021.106239.
85. Bardhan, A., Samui, P., Ghosh, K., Gandomi, A. H., Bhattacharyya, S. (2021). ELM-based adaptive neuro swarm intelligence techniques for predicting the California bearing ratio of soils in soaked conditions. *Applied Soft Computing, 110,* 107595. DOI 10.1016/j.asoc.2021.107595.
86. Kaloop, M. R., Bardhan, A., Kardani, N., Samui, P., Hu, J. W. et al. (2021). Novel application of adaptive swarm intelligence techniques coupled with adaptive network-based fuzzy inference system in predicting photovoltaic power. *Renewable and Sustainable Energy Reviews, 148,* 111315. DOI 10.1016/j.rser.2021.111315.